Journal of Marine Science and Application (2019) 18:492–509
https://doi.org/10.1007/s11804-019-00116-3

RESEARCH ARTICLE

Design and Comparison of H_∞/H_2 Controllers for Frigate Rudder Roll Stabilization

Lijun Wang[1] · Nikolaos I. Xiros[2] · Eleftherios K. Loghis[3]

Received: 27 December 2018 / Accepted: 6 May 2019 / Published online: 30 October 2019

Abstract
Roll motion of ships can be distinguished in two parts: an unavoidable part due to their natural movement while turning and an unwanted and avoidable part that is due to encounter with waves and rough seas in general. For the attenuation of the unwanted part of roll motion, ways have been developed such as addition of controllable fins and changes in shape. This paper investigates the effectiveness of augmenting the rudder used for rejecting part of the unwanted roll, while maintaining steering and course changing ability. For this purpose, a controller is designed, which acts through intentional superposition of fast, compared with course change, movements of rudder, in order to attenuate the high-frequency roll effects from encountering rough seas. The results obtained by simulation to exogenous disturbance support the conclusion that the roll stabilization for displacement can be effective at least when displacement hull vessels are considered. Moreover, robust stability and performance is verified for the proposed control scheme over the entire operating range of interest.

Keywords Rudder roll stabilization · H_∞/H_2 Controllers · Frigate

1 Introduction

In the present study, the problem of roll stabilization by exclusive use of the rudder as an anti-roll countermeasure is examined. The idea that makes this technique possible is the spectral separation of the rudder effect on ship motion. Specifically, the low-frequency part of rudder motion may be used for establishing and maintaining ship course, as it influences yaw, while the high-frequency part develops a rolling torque and, in effect, if appropriately employed, may be used for reducing roll.

Before proceeding to the analysis and control system synthesis, a visit to the roll problem and the various ways to eliminate or, at least, reduce it are given. Although roll existed as an issue since the first surface vessels were built, it increased tremendously in importance in the nineteenth century, when the first steel-hull, motor vessels became mainstream. The main reason was the large reduction of the friction coefficient, due to the use of steel instead of wood; this reduced damping of roll motion. Furthermore, the motorization of propulsion turned the sails and mast gear obsolete; however, this gear has proven to provide a positive roll stabilization effect, which was thus eliminated.

The effects of roll are not negligible onboard modern ships as well. Especially onboard naval vessels, nausea attributed to roll motion may reduce crew performance significantly, despite training. This is due to even trivial reasons, such as the need to use one hand for maintaining balance when the vessel is subject to roll motion, or the loss of concentration and mental focus due to nausea distress. In Faltinsen (1990), a more detailed study has been conducted and a classification of the nausea effects to humans has been proposed. Also, some nausea countermeasures are proposed. For example, it has been observed that the nausea effects are significantly reduced at

Article Highlights
- In the present study, the problem of roll stabilization by exclusive use of the rudder as an anti-roll countermeasure is examined.
- The effects of roll are not negligible onboard modern ships as well.
- The work and analysis presented here assess vis-à-vis the application of H_∞ and H_2 robust control theory for linear, time-invariant, multi-input, multi-output systems in state space.
- The results presented concern a fast naval combat ship, specifically a displacement frigate vessel.

✉ Nikolaos I. Xiros
nxiros@uno.edu

[1] School of Navigation, Guangdong Ocean University, Zhanjiang 524088, China

[2] School of Naval Architecture and Marine Engineering, University of New Orleans, New Orleans, LA 70148, USA

[3] School of Electrical and Computer Engineering, National Technical University of Athens, 15780 Zografou, Greece

the centerline and the bow; when constant visual contact with the exterior is available; when an intellectual task distracts the mind from the roll motion. The fact remains, however, that the vast majority experiences great difficulty due to nausea especially when the roll motion obtains circular frequency around 1.07 rad/s. Unfortunately, for most conventional-hull vessels, this value lies in the vicinity of the roll resonance frequency.

Otherwise, a range of other situations occurring specifically onboard naval vessels require enhanced roll stabilization. Such cases include the extension of the utilization of high-cost equipment and weaponry to a broader range of operating conditions. For example, missiles cannot be launched and radars cannot be operational if a certain limit of either roll or pitch oscillatory motion is exceeded. Furthermore, the need, especially when ASW (Anti-Submarine Warfare) operations are performed, for sea-based helicopter (or airplane) support requires roll motion attenuation in both aircraft takeoff and touchdown phases.

Commonly used roll countermeasures include, except Rudder Roll Stabilization (RRS) that is the subject of this work, the use of anti-roll, U-shaped tanks, bilge keels, and active fin stabilizers. The drawbacks and benefits of each one of these techniques can be found in the literature (Fossen 2011; Perez 2005; Roberts 1992). However, for naval vessels, the RRS system has been proposed as a very suitable solution, due to a number of advantages. These include the low acoustic signature of the RRS system and the low spatial requirements, as the idea is based on modifying the existing shipboard steering gear(s). A more decisive factor is cost vs. performance. The main cost component of an RRS system is the installation of a reliable, fast, and accurate steering gear; required speed is in the range of 15–20(°)/s, when a common steering gear, used only for maneuvering, cannot develop speeds larger than 5(°)/s. On the other hand, an active fin stabilizer system, which is the usual evaluation reference for the RRS technique, requires a hydraulic servo for actuating the fin(s) with similar specifications. Furthermore, a typical RRS system used onboard frigates may achieve roll reduction of up to 75% while a fin stabilizer more than 90%. It is mentioned here that both systems demonstrate reduced roll stabilization capacity as ship forward speed is reduced. This fact is one of the major drawbacks of both stabilization systems.

It is necessary before proceeding to the analysis of the problem to distinguish between roll motion and heeling. Heeling is a hydrostatic situation whereas rolling is a dynamic one. Although heeling has an effect on the roll characteristics of a ship, heeling is not due to the sea waves but to the loading conditions of the ship. Therefore, it can be reduced before departure by appropriately ballasting and rearrangement of the loading.

Although RRS remains as a research subject, there are companies such as SKF and Becker Marine Systems that have commercialized the RRS idea, offering solutions for either cargo or naval ships. The work and analysis presented here assess vis-à-vis the application of H_∞ and H_2 robust control theory for linear, time-invariant, multi-input, multi-output systems in state space. The linearization process for the vessel considered is following familiar lines. However, some significant modifications have been introduced including the use of the describing function approach to model the nonlinearities (mainly saturation and rate limitation) for the steering gear driving the actuating rudder. Also, a general framework for the wave disturbance is introduced in the design process for both the H_∞ and the H_2 approaches. This unified framework allows better comparisons and more useful conclusions.

Regarding paper structure: Section 2 begins with the equations that describe the ship motion dynamics. The formulation of an approach for disturbances of motion follows. The section finishes with the provision of models for the steering gear that will be used.

Section 3 begins with the ship model uncertainties, presents the selected vessel for evaluation of the proposed controller, and provides information regarding the selection of the ship nominal advance speed used as reference. It then advances to steering gear uncertainty modeling and specifies the frequencies of the actuating signal. Next, it deals with roll and yaw movements and the disturbances to these induced by waves. It finishes with two sections providing information regarding the control scheme and methodology.

Section 4 describes the synthesis of a controller based on the H_∞ design method of robust control theory.

Section 5 presents results of simulating the presented methods.

Finally, there are two appendixes providing some theoretical background to aid in understanding the paper content. Appendix 1 provides theoretical background for employing describing functions as a mathematical tool for treating nonlinearities. Appendix 2 provides mathematical formulation elements of robust stability and performance treatment for linear systems.

2 Open-Loop System and Exogenous Disturbance Modeling

2.1 Ship Rolling and Coupled Motions Dynamics

The model used for depicting the roll motion dynamics in this work has been developed in the framework of linearized analysis. In specific, although the starting point is the dynamic equation of motion of the vessel in calm sea conditions, linearization is applied on the basis of the small signal assumption. In effect, the state-space equation obtains the following general form (Christensen and Blanke 1986).

$$\frac{\mathrm{d}}{\mathrm{d}t}\begin{bmatrix} v \\ r \\ \psi \\ p \\ \phi \end{bmatrix} = \begin{bmatrix} a_{11} & a_{12} & 0 & a_{13} & a_{14} \\ a_{21} & a_{22} & 0 & a_{23} & a_{24} \\ 0 & 1 & 0 & 0 & 0 \\ a_{31} & a_{32} & 0 & a_{33} & a_{34} \\ 0 & 0 & 0 & 1 & 0 \end{bmatrix} \cdot \begin{bmatrix} v \\ r \\ \psi \\ p \\ \phi \end{bmatrix} + \begin{bmatrix} b_1 \\ b_2 \\ 0 \\ b_3 \\ 0 \end{bmatrix} \cdot \delta_{\mathrm{R}} \qquad (1)$$

In the above, φ is the angular deflection in the sense of roll, $p = \dot{\varphi}$, ψ is the angular deflection in the sense of yaw, $r = \dot{\psi}$, and δ_R is the actual rudder angle; finally, v is the sway velocity. In the above, it is evident that no exogenous disturbance has been included; furthermore, a method to determine the values of the various system matrices elements is needed. The main conclusion, however, that may be derived from the above is that the open-loop system exhibits decoupled dynamics between the yaw-sway and roll motion, provided that the small signal assumption, required for linearization, holds.

A simplified model has been proposed by Van der Klugt (1987) which maintained only the significant interactions between the various ship motions. In the complex frequency Laplace domain, the simplified model is defined by the following transfer functions.

$$\begin{aligned} v'(s) &= \frac{k_{dv}}{1+T_v s}\delta_R(s) \\ \psi(s) &= \frac{1}{(1+T_r s)s}\left[k_{dr}\delta_R(s) + k_{vr}v'(s) + w_\psi(s)\right] \\ \phi(s) &= \frac{{\omega_n}^2}{s^2 + 2\zeta\omega_n s + {\omega_n}^2}\left[k_{dp}\delta_R(s) + k_{vp}v'(s) + w_\phi(s)\right] \end{aligned} \tag{2}$$

Van Amerongen et al. (1990) have shown that the above model is of enhanced value for autopilot and RRS system designs. Furthermore, note that this simplified model contains wave-induced disturbances in both the roll and yaw senses of motion, termed w_φ and w_ψ, respectively. Finally, the sway velocity v has been replaced by a new variable v', which is the sway velocity component due to exclusively rudder activity. A drawback, however, is that this variable is not directly measurable but can be deduced from measurements only by use of a state observer, e.g., a Kalman filter. The open-loop transfer functions of Eq. (2) may be converted to the following state-space expression in the time domain.

$$\begin{aligned} \frac{\mathrm{d}}{\mathrm{d}t}\begin{bmatrix} v' \\ p \\ \varphi \\ r \\ \psi \end{bmatrix} &= \begin{bmatrix} -\frac{1}{T_v} & 0 & 0 & 0 & 0 \\ \omega_n^2 k_{vp} & -2\zeta\omega_n & -\omega_n^2 & 0 & 0 \\ 0 & 0 & 0 & 0 & 0 \\ \frac{k_{vr}}{T_r} & 0 & 0 & -\frac{1}{T_r} & 0 \\ 0 & 0 & 0 & 1 & 0 \end{bmatrix}\begin{bmatrix} v' \\ p \\ \varphi \\ r \\ \psi \end{bmatrix} + \\ &\quad \begin{bmatrix} \frac{k_{dv}}{T_v} \\ \omega_n^2 k_{dp} \\ 0 \\ \frac{k_{dr}}{T_r} \\ 0 \end{bmatrix}\delta_R + \begin{bmatrix} 0 & 0 \\ \omega_n^2 & 0 \\ 0 & 0 \\ 0 & \frac{1}{T_r} \\ 0 & 0 \end{bmatrix}\begin{bmatrix} \omega_\varphi \\ \omega_\varphi \end{bmatrix} \Leftrightarrow \\ &\quad \dot{\chi} = A\chi + B\delta_R + \phi\omega \end{aligned} \tag{3}$$

$$\begin{aligned} &U\ [\mathrm{m/s}], T_v\ [\mathrm{s}] = \frac{78}{U}, T_r\ [\mathrm{s}] = \frac{13}{U}, \\ &\omega_n\ [\mathrm{rad/s}] = 0.63, \zeta[-] = 0.064 + 0.0038U, \\ &k_{vr}\ [(^\circ)/\mathrm{m}] = -0.46, k_{dr}\ [\mathrm{Hz}] = -\frac{0.0027}{U}, \\ &k_{dp}\ \left[1/\mathrm{rad}^2\right] = -0.0014U^2, \\ &k_{dv}\ [\mathrm{m}/(\mathrm{s}\cdot(^\circ))] = 0.01U, \\ &k_{vp}\ \left[(\mathrm{s}\cdot(^\circ))/(\mathrm{m}\cdot\mathrm{rad}^2)\right] = 0.21U \end{aligned} \tag{4}$$

$$\begin{aligned} \boldsymbol{A}_0 &= \begin{bmatrix} -0.0989 & 0 & 0 & 0 & 0 \\ 0.6432 & -0.1176 & -0.3969 & 0 & 0 \\ 0 & 1 & 0 & 0 & 0 \\ -0.2731 & 0 & 0 & -0.5937 & 0 \\ 0 & 0 & 0 & 1 & 0 \end{bmatrix} \\ \boldsymbol{A}_U &= \begin{bmatrix} -0.0989 & 0 & 0 & 0 & 0 \\ 0.6432 & -0.0043512 & 0 & 0 & 0 \\ 0 & 1 & 0 & 0 & 0 \\ -0.2731 & 0 & 0 & -0.5937 & 0 \\ 0 & 0 & 0 & 1 & 0 \end{bmatrix} \\ \boldsymbol{B}_0 &= \begin{bmatrix} 0.00764 \\ -0.03310 \\ 0 \\ -0.00021 \\ 0 \end{bmatrix}, \boldsymbol{B}_U = \begin{bmatrix} 0.01527 \\ -0.06620 \\ 0 \\ -0.00042 \\ 0 \end{bmatrix} \\ \boldsymbol{\Phi}_0 &= \begin{bmatrix} 0 & 0 \\ 0.3969 & 0 \\ 0 & 0 \\ 0 & 0.5937 \\ 0 & 0 \end{bmatrix}, \boldsymbol{\Phi}_U = \begin{bmatrix} 0 & 0 \\ 0 & 0 \\ 0 & 0 \\ 0 & 0.5937 \\ 0 & 0 \end{bmatrix} \end{aligned} \tag{5}$$

Both in the above expression and more prominently in the transfer functions introduced in Eq. (2), the spectral separation between the yaw/sway dynamics and the roll motion dynamics is clearly manifested, at least as far linearized analysis is concerned. Indeed, the scalar transfer functions involved in the yaw/sway motions obtain low-frequency pole(s) while the one involved in roll demonstrates the typical structure of the second-order linear oscillator. This fact lies at the heart of the RRS concept.

2.2 Wave Disturbance Modeling

The standard practice to model the wave field acting on a floating vessel as a stochastic process is pursued in this work (Van der Klugt 1987; Fossen 1994; Lauvdal 1998). According to this approach, a power spectral density (PSD) characterizes the frequency spectrum of the sea waves, i.e., the Fourier transform of the autocorrelation function of the free surface elevation, when integrated over all wave directions. A wide variety of such PSD functions has been proposed. The most popular are these formulated by Neumann (1952), Bretschneider (1959), Pierson and Moskowitz (1964). The latter two bear significant similarities as they were conceived on the basis of data for fully developed, wind generated seas in the North Atlantic Ocean. The mathematical expression for the PSD according to Pierson and Moskowitch is given by the following.

$$S(\omega) = A_g\omega^{-5}\exp\left(-B_{wv}\omega^{-4}\right) \quad \left[\mathrm{m}^2\cdot\mathrm{s}\right] \tag{6}$$

In the above, A_g and B_{wv} are constants; A_g depends exclusively on the gravity constant, g, whereas B_{wv} is determined by the wind speed. By adopting the additional assumption that

the sea waves may be modeled as a narrow-band Gaussian stochastic process, constant B_{wv} may be linked to significant wave height, H_s. In SI units, the following relationships hold for these two constants (Faltinsen 1990; Fossen 2011).

$$A_g = 0.0081g^2 = 0.78, B_{wv} = {}^{3.14}/_{H_s^2} \tag{7}$$

Furthermore, the modal frequency, i.e., the frequency at which the maximum of the PSD is observed may be determined as the root of the derivative of $S(\omega)$.

$$\frac{\mathrm{d}}{\mathrm{d}\omega}S(\omega) = 0 \Rightarrow \omega_0 = \sqrt[4]{\frac{4B_{wv}}{5}} \tag{8}$$

The above results have been used in order to construct a rational approximation of the above sea wave spectrum. In specific, the transfer function of a strictly proper, realizable, linear, and time-invariant system is sought after. The main requirement of such a transfer function is that, when driven by white Gaussian noise, it generates a colored Gaussian noise response whose PDF approximates, in some sense, the one in Eq. (6).

A variety of such transfer functions has been proposed in the literature (Balchen et al. 1980; Saelid and Jenssen 1983; Triantafyllou et al. 1983; Fossen 1994). The prominent common characteristic of all is their band-pass nature which comes as a consequence of the narrow-band shape of the PDF in Eq. (6). However, as the expression in Eq. (6) is irrational, it is expected that by increasing the order of the approximating transfer function, the accuracy of approximation will be increased; for example, in Triantafyllou et al. (1983), a 6th-order transfer function is proposed. However, for robust control purposes, a rougher approximation is sufficient. Therefore, a resonant 2nd-order transfer function, as in Saelid and Jenssen (1983) and Fossen (1994), is selected for modeling the sea wave disturbance generation.

$$\begin{aligned} h_w(s) &= \frac{k_w s}{s^2 + 2\zeta_w\omega_0 s + {\omega_0}^2} \overset{s=j\omega}{\Rightarrow} \\ |h_w(\omega)| &= \frac{k_w\omega}{\sqrt{\left({\omega_0}^2-\omega^2\right)^2 + \left(2\zeta_w\omega_0\omega\right)^2}} \end{aligned} \tag{9}$$

By using the above, the following may be obtained.

$$\|h_w(\omega)\|_\infty \triangleq \sup_{\omega\geq 0}|h_w(\omega)| = |h_w(\omega_0)| = \frac{k_w}{2\zeta_w\omega_0} \tag{10}$$

Commonly, for convenience, constant k_w is set equal to the quantity $(2\zeta_w\omega_0)$ and, therefore, $\|h_w(\omega)\|_\infty = 1$. If the above system is driven by zero-mean, white Gaussian noise of unity standard deviation, the output will be a narrow-band, colored, Gaussian, stochastic process with PSD $|h_w(\omega)|^2$. For robust control synthesis purposes, it is sufficient that the peak value of the wave model in Eq. (9) is equal to the one given by the non-parametric spectrum of Eq. (6). In the case that the driving white noise standard deviation is not unity, but $\sigma_w \neq 1$, the following is obtained.

$$\sigma_w^2 = S(\omega_0) = A_g \mathrm{e}^{-1.25}{\omega_0}^{-5} \quad \left[\mathrm{m}^2\cdot\mathrm{s}\right] \tag{11}$$

Note that the roll-off characteristics of the wave spectrum are not adequately modeled through the use of the second-order model of Eq. (9). However, as explained later, this modeling simplification may be overcome by employing robust control theory.

Another aspect of concern when designing a control system for roll motion mitigation is the encounter frequency. When the vessel moves towards a certain direction, conventionally referred to as forward direction, with constant average speed, the wave frequency experienced shipboard, referred to as encounter frequency, differs from the one measured at the fixed reference frame. The calculation of the encounter frequency is based on the Doppler effect experienced by a moving wave receiver.

$$\omega_e = \omega_0 - {\omega_0}^2\frac{U}{g}\cos\beta_w \tag{12}$$

In the above, U is the ship's average forward speed, g the gravity constant, and β_w is the so-called encounter angle of the waves by the ship ($0 \leq \beta_w \leq \pi$ with zero corresponding to following seas). The way to deal with this problem in a robust control framework is to use a weighting filter that allows a variable resonance frequency, by considering it as uncertain.

2.3 Steering Gear Modeling

The steering gear in an RRS system is the control system actuator for both the conventional autopilot course-keeping function and the active stabilization system (Fig. 1). The limitations imposed by a slow and/or inaccurate to the tuning of the control law are analyzed later. At this point, however, the model of a hydraulic steering gear, suitable for the controller synthesis task, needs to be presented.

A common way to model the effect of a linear, noiseless actuator, without the need to employ a detailed physical model, is a first-order transfer function of the form given below (Golnaraghi and Kuo 2010).

$$N_{steer}(\omega, A_\delta, 0) = \begin{cases} 1, 0 < A_\delta < \delta_{\mathrm{LIM}} \\ \frac{2}{\pi}\left[\frac{\arcsin\left(\frac{\delta_{\mathrm{LIM}}}{A_\delta}\right) + {}^{\delta}\mathrm{LIM}}{A_\delta}\sqrt{1-\left(\frac{\delta_{\mathrm{LIM}}}{A_\delta}\right)^2}\right], A_\delta \geq {}^{\delta}\mathrm{LIM} \end{cases} \frac{1}{\mathrm{j}\omega\tau + 1} \tag{13}$$

A variety of methods exists for determining the time constant of the model shown above, mainly in system identification literature (Christensen and Blanke 1986; Cowley and

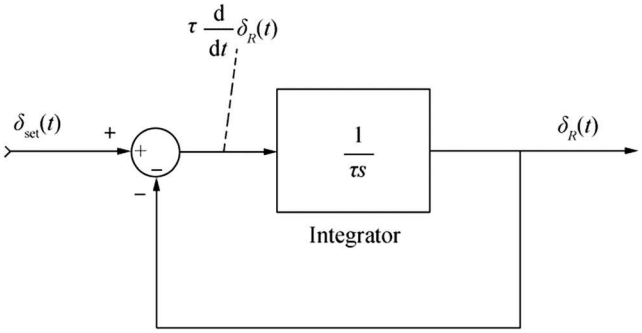

Fig. 1 Linear actuator model used for the steering gear

Lambert 1972; Eda and Crane 1965; Fossen 2011; Healey 1992; Perez 2005; Smith 1977; SNAME 1989; Son and Nomoto 1981; Van Amerongen and Van Cappelle 1981; Zhou 1987). The central idea is to drive the actuator with either deterministic or deterministic small amplitude signals, in order for the linearity to be preserved, and study the response mainly in terms of cross-correlation with the input signal. On the other hand, the transfer function structure is better manifested in the manipulated form given in the last of the equations in Eq. (13). In this form, the transfer function takes the negative feedback form of Fig. 2.

In typical marine hydraulic steering gears, two major nonlinearities appear that make the predictions of the transfer function model of Eq. (13) rather inaccurate in both in terms of timing and of amplitude, when large and/or rapid transients arise. The first has to do with the capacity of the feeding pump(s) providing the hydraulic power required for actuation. The fact that this capacity is finite sets an upper limit to the turning (rotational) speed that can be achieved by the gear; in effect, the value of $|\dot{\delta}_R(t)|$ cannot be arbitrarily large. The second nonlinearity is the one connected with the rudder angle of deviation with respect to the vessel's centreline; this is limited commonly somewhere between 35 and 40 degrees. Note that this feature is rather universal for all ships. In effect, $|\dot{\delta}_{set}(t)|$ must be limited. Note that a linear controller does not provide with an inherent capability of saturating its output; therefore, the control signal has to be saturated externally. By introducing these two nonlinearities in the transfer

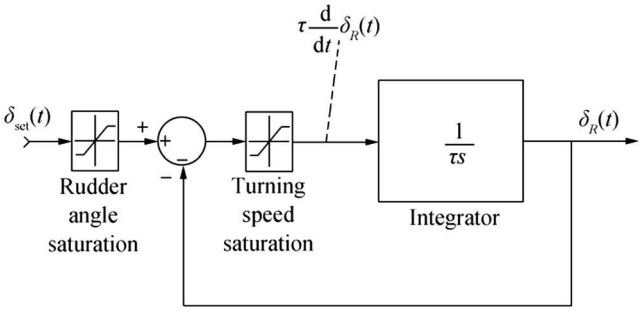

Fig. 2 Model with transfer function and saturation nonlinearities used for the steering gear

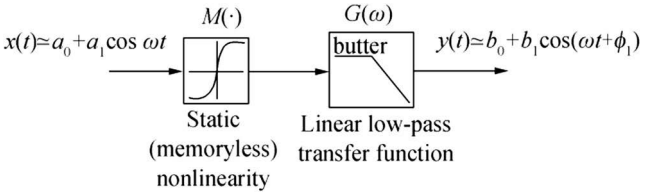

Fig. 3 Feedthrough system with static nonlinearity followed by low-pass transfer function

function model shown in Fig. 2, the one shown in Fig. 3 is obtained.

3 Formulation of the Robust Control Problem

3.1 Ship Model Uncertainty Characterization

The ship model introduced in Eq. (3) contains a number of coefficients. These coefficients may be determined by either tank model experiments or sea trials or hydrodynamic calculations (numerical or analytic). In any case, however, their value will not be constant; commonly, they can be parameterized on the basis of a small number of major operational variables. In most analyses, the vessel's mean forward advance speed, U, is included in such a parameterization.

Although intuitively, such dependence or trends are expected; the fact is that a universally valid mathematical expression may not be in general assumed. On the other hand, for a given vessel, curve-fitting techniques may be employed, in order to yield empirical relationships between the coefficients in the linearized state-space model of Eq. (3) and mean advance speed U.

In this work, a Dutch, M-type frigate was used as a test case. The first reason for this choice was that the effect roll is more prominent on naval vessels, especially high-speed ones with considerable maneuverability requirements such as frigates. A second reason was that the Hellenic Navy has expressed interest in acquiring a number of vessels of this type during the mid 1980s. Although finally the German MEKO-200 design has been selected, the two designs bear significant similarities. Furthermore, the Dutch M-type was one of the first frigate types to be fitted with an RRS system. Another frigate type, with similar characteristics to the M one, fitted with an RRS system was the German F-124. Actually, the RRS system was one of the main differences between the F-124 and its predecessor F-123; the F-123 was equipped with a more conventional active fin stabilization system.

The main reason for choosing the M-type frigate as the test case in this work, however, is the fact that several pieces of

literature can be found concerning its RRS system technical specification (Kallstrom and Schultz 1990; Lloyd 1975; Roberts 1992; Sorensen et al. 1995; Smith 1977; SNAME 1989; Son and Nomoto 1981). Therefore, the ship's main particulars and, more important, the values of the coefficients in Eq. (3) may easily be determined. Furthermore, the performance achieved by the proposed RRS system controller may be assessed against the one obtained by alternative controller synthesis methods in a straightforward manner.

In this respect, the dependence of the model coefficients in Eq. (3) on the ship's advance speed has been quantified in the following semi-empirical formulae (Kallstrom and Schultz 1990; Lloyd 1975; Roberts 1992; Sorensen et al. 1995; Smith 1977; SNAME 1989; Son and Nomoto 1981):

$$\begin{aligned}
&U\ [\mathrm{m/s}], T_v\ [\mathrm{s}] = \frac{78}{U}, T_r\ [\mathrm{s}] = \frac{13}{U},\\
&\omega_n\ [\mathrm{rad/s}] = 0.63,\\
&\zeta\ [-] = 0.064 + 0.0038U,\\
&k_{vr}\ [(^\circ)/\mathrm{m}] = -0.46,\\
&k_{dr}\ [\mathrm{Hz}] = -\frac{0.0027}{U},\\
&k_{dp}\ \left[1/\mathrm{rad}^2\right] = -0.0014U^2,\\
&k_{dv}\ [\mathrm{m}/(\mathrm{s}\cdot(^\circ))] = 0.01U,\\
&k_{vp}\ \left[(\mathrm{s}\cdot(^\circ))/\left(\mathrm{m}\cdot\mathrm{rad}^2\right)\right] = 0.21U
\end{aligned} \tag{14}$$

The above formulae have been employed in the design stages of the first operational RRS system by the Royal Netherlands Navy and have been deduced through campaigns of scale model experiments as well as field measurements. In the end of porting the above relationships to the standard form in the robust controller synthesis literature, the forward speed of $U_0 = 15$ kn = 7.7175 m/s will be considered the nominal advance speed of the vessel. Such speed is in the range of typical service speeds for various naval vessels such as frigates and destroyers. Finally, it is noted that the range of forward speed, U, for which RRS is intended to be employed spans the range between 5 kn (2.5725 m/s) and 25 kn (12.8625 m/s).

This speed value will be used for the calculation of the nominal system matrices in Eq. (3) and the nominal transfer function coefficients in Eq. (2). Specifically, the system matrices are expressed as follows.

$$\begin{aligned}
&\boldsymbol{A} = \boldsymbol{A}_0 + \Delta U\cdot\boldsymbol{A}_U,\\
&\boldsymbol{B} = \boldsymbol{B}_0 + \Delta U\cdot\boldsymbol{B}_U,\\
&\boldsymbol{\Phi} = \boldsymbol{\Phi}_0 + \Delta U\cdot\boldsymbol{\Phi}_U,\\
&\Delta U \triangleq \frac{U-U_0}{U_0} \Rightarrow\\
&\frac{5-15}{15} = -\frac{2}{3} \le \Delta U \le \frac{25-15}{15} = \frac{2}{3}
\end{aligned} \tag{15}$$

The numerical values of nominal matrices $\boldsymbol{A}_0$,$\boldsymbol{B}_0$, and $\boldsymbol{\Phi}_0$ as well as the uncertainty coefficient matrices $\boldsymbol{A}_U$,$\boldsymbol{B}_U$, and $\boldsymbol{\Phi}_U$ are calculated on the basis of numerical formulae (14) using the value of $\boldsymbol{U}_0$ and finally substitution in Eq. (3). Also, as readily verified above, the uncertainty in forward speed is bounded, i.e., $|\Delta \boldsymbol{U}| < 0.667$.

$$\begin{aligned}
\boldsymbol{A}_0 &= \begin{bmatrix} -0.0989 & 0 & 0 & 0 & 0\\ 0.6432 & -0.1176 & -0.3969 & 0 & 0\\ 0 & 1 & 0 & 0 & 0\\ -0.2731 & 0 & 0 & -0.5937 & 0\\ 0 & 0 & 0 & 1 & 0 \end{bmatrix}\\
\boldsymbol{A}_U &= \begin{bmatrix} -0.0989 & 0 & 0 & 0 & 0\\ 0.6432 & -0.0043512 & 0 & 0 & 0\\ 0 & 1 & 0 & 0 & 0\\ -0.2731 & 0 & 0 & -0.5937 & 0\\ 0 & 0 & 0 & 1 & 0 \end{bmatrix}\\
\boldsymbol{B}_0 &= \begin{bmatrix} 0.009086\\ -0.03938\\ 0\\ -0.01474\\ 0 \end{bmatrix}\\
\boldsymbol{B}_U &= \begin{bmatrix} 0.018172\\ -0.07876\\ 0\\ -0.02948\\ 0 \end{bmatrix}\\
\boldsymbol{\Phi}_0 &= \begin{bmatrix} 0 & 0\\ 0.3969 & 0\\ 0 & 0\\ 0 & 0.5937\\ 0 & 0 \end{bmatrix}\\
\boldsymbol{\Phi}_U &= \begin{bmatrix} 0 & 0\\ 0 & 0\\ 0 & 0\\ 0 & 0.5937\\ 0 & 0 \end{bmatrix}
\end{aligned} \tag{16}$$

In the above, units have been omitted for the sake of simplicity.

3.2 Steering Gear Uncertainty and Nonlinearity Characterization

The main source of uncertainty in the hydraulic steering gear modeling comes from linearization. Indeed, in order to employ a variant of the linear robust controller design theory, linearization of the actuator dynamics is a prerequisite. However, due to the fact that the nonlinearities involved belong to the hard type (saturations) standard linearized analysis, through Taylor expansion and elimination of terms with order higher than one is of limited value. Such an approach cannot reveal the possible effects due to the steering gear nonlinearities.

In order to avoid the above limitation, an alternative methodology of linearization is employed, based on the describing function. In the literature (Nagrath and Gopal 1986; Smith 1977; Zhou 1987), the describing function is introduced in the purpose of linearization in the frequency domain, of open or closed-loop systems with dynamic or static nonlinearities at the feedforward or feedback path. However, a requirement for the applicability of the analysis with the describing function approach is that the output signal of the nonlinear system is the response of a linear low-pass filter. This filter mitigates higher-order harmonics from the output signal that might be generated by the nonlinearities present either in the feedforward or in the feedback path.

Coming back to Fig. 3, it is easily seen that this condition is met by the nonlinear steering gear model employed. Indeed, the first-order linear filter, due to the small signal, linear steering gear dynamics, plays this role. As mentioned in Appendix 1, the describing function technique consists of linearization in the frequency domain by neglecting the higher-order harmonics of the response, provided that an output low-pass filter is present. This frequency domain linearization is practically implemented by assuming sinusoidal inputs of various frequencies. In the case of the steering gear model of Fig. 3, and by neglecting the turning rate limiter, it can be seen that the steering gear linear dynamics are given by Eq. (13). In effect, with respect to Eqs. (A.6) and (A.7), the describing function of the steering gear with the turning rate limiter nonlinearity excluded assumes the following form.

$$\left\{\begin{array}{c} N_{steer}(\omega,A_\delta,0)= \\ 1,\,0<A_\delta<\delta_{\mathrm{LIM}} \\ \frac{2}{\pi}\left[\frac{\arcsin\left(\frac{\delta\mathrm{LIM}}{A_\delta}\right)+{}^{\delta}\mathrm{LIM}\sqrt{1-\left(\frac{\delta\mathrm{LIM}}{A_\delta}\right)^2}}{A_\delta}\right],A_\delta\geq{}^{\delta}\,\mathrm{LIM} \end{array}\right\}\frac{1}{\mathrm{j}\omega\tau+1} \tag{17}$$

In the above, δ_{LIM} is the limiter saturation value, which as said, lies commonly between 35 and 40 degrees; A_δ is the amplitude and ω the frequency of the command signal as follows.

$$\delta_{\mathrm{set}}(t)=A_\delta\cos\omega t=\mathrm{Re}\left\{A_\delta \mathrm{e}^{\mathrm{j}\omega t}\right\} \tag{18}$$

The describing function in Eq. (17) may be rewritten as a product of a variable, uncertain gain and the linear dynamics of the steering gear. In this form, the describing function is a linear, but uncertain, transfer function.

$$\begin{aligned} &N_{\mathrm{steer}}(\omega,A_\delta,0)=k_{\mathrm{R}}(A_\delta)\cdot\frac{1}{\mathrm{j}\omega\tau+1}\Rightarrow \\ &N_{\mathrm{steer}}(\omega,A_\delta,0)=[k_{\mathrm{R0}}+\delta k_R(A_\delta)]\cdot\frac{1}{\mathrm{j}\omega\tau+1} \end{aligned} \tag{19}$$

The block diagram of this steering gear dynamic representation is given in Fig. 4. It is noted here that the describing function introduced and used in this text represents the linearized, in the frequency domain, steering gear dynamics for a sinusoidal input. However, this suffices in the case of anti-roll

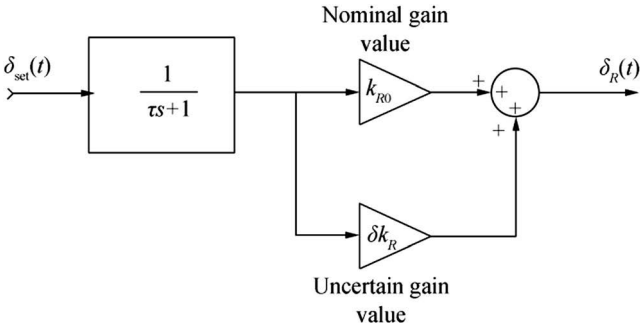

Fig. 4 Uncertain linear model used for the steering gear

action using RRS systems, because the disturbance signal is a waveform commonly sinusoidal, or very close to that. Indeed, the sea wave disturbance model to be used is the 2nd-order, resonant transfer function of Eq. (9), which as argued gives rise to a narrow-band Gaussian stochastic process. This narrow-band stochastic signal generates the ship roll motion, when propagated through the linearized dynamics of Eq. (3). The vessel's roll motion, in turn, drives the RRS system controller which is also a linear system. Therefore, the control signal may be expected to be a close to sinusoidal waveform of frequency equal to that of the disturbance. This argumentation supports the use of the sinusoidal input describing function.

In order to calculate the nominal value, δk_{R0}, and the range of the uncertainty, δk_{R0}, of the gain in Eq. (19), the range of amplitude A is needed. As the motion of the steering gear is rotary, it is evident that the values of the command signal, δ_{set}, is wrapped in an interval with width 2π radians, e.g., interval $(-\pi, \pi]$; therefore, in degrees, the maximum absolute value of A_δ is 180°. Furthermore, for the calculations below, it is assumed that $\delta_{\mathrm{LIM}}=35°$.

$$\begin{aligned} &k_{\mathrm{R}}(180°)=0.2460\leq k_{\mathrm{R}}(A_\delta)\leq 1 \\ &k_{R0}=\frac{1+0.2460}{2}=0.6230 \\ &|\delta k_{\mathrm{R}}|\leq\frac{1-0.2460}{2}=0.3770 \end{aligned} \tag{20}$$

In order to take into account the turning rate limitations of an actual steering gear, which have been omitted from the describing function above, inclusion of the turning rate in the cost function, involved in any optimal control synthesis method, suffices if combined with a high-pass filter, penalizing gravely the high-frequency spectral content of the command signal, δ_{set}. Indeed, if such a technique is adopted, the resulting controller practically is driven to generate low-frequency control signals.

A common choice for analog or digital filters in a variety of engineering applications is that of Butterworth filters. The main advantage of these filters is the maximally flat amplitude frequency response demonstrated in the pass band and, in general, smooth and monotonic amplitude frequency response. In order to achieve maximal flatness, however, one has to sacrifice roll-off steepness. Thus, a Chebyshev or

elliptic filter of the same order demonstrates much steeper roll-off characteristic than their Butterworth counterpart.

In the case examined here, the steering gear turning rate filter synthesis was based on a cascaded interconnection of two third-order, high-pass Butterworth filters.

$$\begin{aligned} H_{B,3,\mathrm{hp}}(s) &= \frac{1}{\left(\frac{\omega_c}{s}\right)^3 + 2\left(\frac{\omega_c}{s}\right)^2 + 2\left(\frac{\omega_c}{s}\right) + 1} \Leftrightarrow \\ H_{B,3,\mathrm{hp}}(s) &= \frac{s^3}{s^3 + 2\omega_c s^2 + 2\omega_c{}^2 s + \omega_c{}^3} \Leftrightarrow \\ H_{B,3,\mathrm{hp}}(s) &= \frac{s^3}{(s+\omega_c)(s^2 + \omega_c s + \omega_c{}^2)} \end{aligned} \tag{21}$$

The cutoff frequency of the first filter is 0.25 rad/s ≈ 14 (°)/s and of the second one is 0.26 rad/s ≈ 15 (°)/s. These values have been selected in accordance with turning rate values achieved by steering gears already in service onboard naval vessels equipped with RRS systems (Cowley and Lambert 1972; Fossen 2011; Kallstrom and Schultz 1990; Lloyd 1975; Perez 2005; Son and Nomoto 1981; Van Amerongen and Van Cappelle 1981). However, in order to moderate the effect of the triple zero at $s = 0$ demonstrated by high-pass Butterworth filters, the zeros have been relocated slightly on the negative real semi-axis. The transfer functions of the filters, as finalized after fine tuning and trial-and-error, are given below.

$$\begin{aligned} H_{\mathrm{steer},1}(s) &= \frac{(s+0.005)(s+0.007)(s+0.009)}{(s+0.25)(s^2+0.25s+0.0625)} \\ H_{\mathrm{steer},2}(s) &= \frac{(s+0.004)(s+0.006)(s+0.008)}{(s+0.26)(s^2+0.26s+0.0676)} \end{aligned} \tag{22}$$

By combining the above and incorporating a penalization gain of 500 for exceeding the turning rate of 15 (°)/s, the following performance weighting filter for the control signal is obtained.

$$\begin{aligned} H_{\mathrm{steer},0}(s) = \\ 500 \cdot \frac{s^3 + 0.021s^2 + 1.43\times10^{-4}s + 3.15\times10^{-7}}{s^3 + 0.5s^2 + 0.1252s + 0.01568} \cdot \\ \frac{s^3 + 0.018s^2 + 1.04\times10^{-4}s + 1.92\times10^{-7}}{s^3 + 0.52s^2 + 0.1351s + 0.01756} \end{aligned} \tag{23}$$

The amplitude Bode plot, i.e., the amplitude frequency characteristic, of $H_{\mathrm{steer}}(s)$ is shown in Fig. 5. The incorporation of the control signal, δ_{set}, weighted by the filter above, in the cost function, during controller synthesis leads to control law gains that do not emphasize high frequencies; therefore, the requirement for maintaining steering gear turning rate below a specified threshold is met.

3.3 Roll and Yaw Weighted Performance

As was the case for the steering control action, the roll and yaw performance must, also, be properly weighted

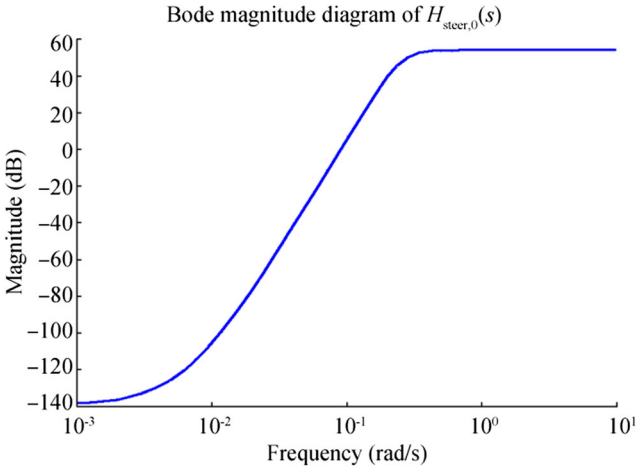

Fig. 5 Weight filter applied to the steering control action

before contributing to the optimal control cost function. However, in this case, the fact that these signals are outputs of the open-loop system, instead of inputs, has to be taken into account. By combining the relationships in Eq. (2) with the one in Eq. (9), the following expression is obtained for the roll and yaw motions due to wave disturbance only.

$$\begin{aligned} \psi_w(s) &= H_{W,\psi}(s)\cdot w_\psi(s) = \frac{1}{s(1+T_r s)}\cdot w_\psi(s) \Rightarrow \\ \psi_w(s) &= \frac{1}{1+T_r s}\cdot\frac{2\zeta_w\omega_0\sigma_{w,\psi}}{s^2+2\zeta_w\omega_0 s+\omega_0{}^2}\cdot w_{G,1} \\ \phi_w(s) &= H_{W,\phi}(s)\cdot w_\phi(s) = \frac{\omega_n{}^2}{s^2+2\zeta\omega_n s+\omega_n{}^2}\cdot w_\phi(s) \Rightarrow \\ \phi_w(s) &= \frac{\omega_n{}^2}{s^2+2\zeta\omega_n s+\omega_n{}^2}\cdot\frac{2\zeta_w\omega_0\sigma_{w,\phi}s}{s^2+2\zeta_w\omega_0 s+\omega_0{}^2}\cdot w_{G,2} \end{aligned} \tag{24}$$

In the above, $\sigma_{w,\psi}$ and $\sigma_{w,\phi}$ are the standard deviations of the white noise signals driving the wave models for yaw and roll, respectively. In general, their values are different. However, the maximum values expected for these parameters may be assumed equal. Furthermore, the wave model parameters ω_0 and ζ_w are expected to assume the same value for both yaw and roll. The vector $\boldsymbol{w}_G = [w_{G,1}\ w_{G,2}]^{\mathrm{T}}$ consists of two scalar, mutually independent, white, Gaussian stochastic processes of zero mean and unity standard deviation.

Also, note that the zero at $s = 0$ appearing in the wave model for yaw, $w_\psi(s)$, is canceled due to the pure integrator of the yaw motion dynamics.

The expressions in Eq. (24) can be used in order to estimate the scaling factors needed for optimal control synthesis. As in the case of the steering gear turning rate, the values of yaw and roll deflection have to be scaled (normalized) before contributing to the cost function associated with the performance of the optimal control system. Although the colored disturbance inputs are expected to assume the same maximum frequency

response value, i.e., $\|w_\psi(s)\|_\infty = \|w_\phi(s)\|_\infty$, in general, it will hold that $\|\psi(s)\|_\infty \neq \|\phi(s)\|_\infty$. This is due to the fact that they propagate through different transfer functions. Therefore, they may contribute in a distorted manner to the value of the optimal control cost function. In conclusion, the following scaling needs to be applied to the yaw and roll outputs.

$$\begin{aligned}\psi_\varnothing &= \frac{1}{\left|\frac{1}{j\omega_{0,\min}\left(1+T_r\, j\omega_{0,\min}\right)}\right|}\cdot\psi \Leftrightarrow \\ \psi_\varnothing &= \omega_{0,\min}\sqrt{1+T_r^2\omega_{0,\min}^2}\cdot\psi \\ \phi_\varnothing &= \frac{1}{\left|\frac{1}{2\zeta}\right|}\cdot\phi = 2\zeta\cdot\phi\end{aligned} \tag{25}$$

As can be seen, variables $\psi_\varnothing$, $\phi_\varnothing$ are the scaled yaw and roll, respectively, to be used in the optimal control cost function. The rationale of the scaling weights applied is based on Eq. (24) and the form of the spectrum of the driving wave disturbances w_ψ, w_ϕ.

For the yaw variable, the zero-pole cancelation at $s = 0$ allows to select a purely positive frequency value where the yaw transfer function, $H_{W,\psi}(s)$, assumes a finite value. In order to choose the appropriate frequency value, one has to take into account the minimum frequency at which the wave spectrum may demonstrate a peak. As seen in Fig. 6, the resonance frequency of the wave spectrum for significant wave height of 10 m is no less than 0.3 rad/s. Here, it is noted that the probability to observe waves with significant wave height 10 m or above has been reported to less than 2%; furthermore, the wave PSD peak value increases for decreasing resonance frequency, as a consequence of the significant wave height.

However, in order to account for the encounter frequency, as calculated in Eq. (12), the frequency value $\omega_{0,\min}$ is calculated as follows.

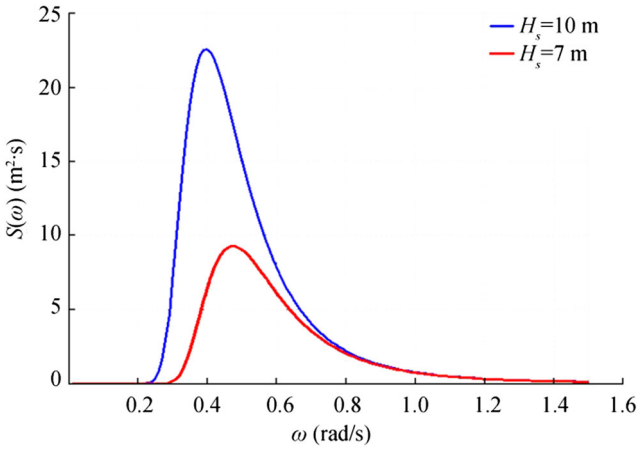

Fig. 6 Pierson-Moskowitch sea wave PSDs for two significant wave heights (denoted by H_s)

$$\begin{aligned}\omega_{0,\min} &= 0.3\ \text{rad/s} - (0.3\ \text{rad/s})^2 \times \frac{12.8625\ \text{m/s}}{9.81\ \text{m/s}^2} \times 1 \Leftrightarrow \\ \omega_{0,\min} &= 0.1820\ \text{rad/s}\end{aligned} \tag{26}$$

The speed value used in the above is the maximum within the vessel's operational envelope, i.e., equal to (U_0 + max ΔU). On the other hand, the nominal speed value is used for the calculation of time constant T_r according to Eq. (14), without major loss in accuracy. Note that, because the selected $\omega_{0,\ \min}$ is rather small, the effect of this time constant on accuracy is rather limited as can be seen from Eq. (25).

For the roll variable, it can be seen that the relative transfer function,$H_{W,\ \varphi}(s)$, assumes finite values for every frequency ω. Thus, the straightforward choice for the scaling factor is $\|H_{W,\varphi}(s)\|_\infty^{-1} = |H_{W,\varphi}(j\omega_n)|^{-1}$. For this calculation, the value of the damping coefficient ζ is set to the one calculated by using the minimum speed value, (U_0 + min ΔU), in the related expression of Eq. (14). By employing the above, the following scaling formulae are deduced.

$$\psi_\varnothing = 0.1904\cdot\psi,\ \phi_\varnothing = 0.1476\cdot\phi \tag{27}$$

3.4 The Full Control Model

By combining the aforementioned elements, the control model of the naval vessel at hand with autopilot and RRS system, shown in Fig. 6, is constructed. As can be seen, the output of the model is the weighted yaw and roll performance as well as the weighted control action, i.e., $\delta_{R,\ \varnothing}$. These are the variables that will contribute to the optimal control cost function during the controller synthesis method. In the figure, matrix $\boldsymbol{C}_0$ is defined as follows.

$$\boldsymbol{C}_0 = \begin{bmatrix} 0 & 0 & 0.1476 & 0 & 0 \\ 0 & 0 & 0 & 0 & 0.1904 \end{bmatrix} \tag{28}$$

Also, note that matrices $\boldsymbol{A}$, $\boldsymbol{B}$, and $\boldsymbol{\Phi}$ are uncertain as specified in Eq. (15). Furthermore, gain $\boldsymbol{k_R}$ is uncertain according to Eq. (20).

The system shown in Fig. 6 is closed-loop. Therefore, matrix $\boldsymbol{C}$ is determining which components of the state vector $\boldsymbol{x}$, as defined in Eq. (3), are available for real-time

$$\boldsymbol{C} = \boldsymbol{I}_5 = \begin{bmatrix} 1 & 0 & 0 & 0 & 0 \\ 0 & 1 & 0 & 0 & 0 \\ 0 & 0 & 1 & 0 & 0 \\ 0 & 0 & 0 & 1 & 0 \\ 0 & 0 & 0 & 0 & 1 \end{bmatrix} \tag{29}$$

As can be seen, due to the employment of gyrocompasses and GPS, all yaw and roll deflection angles, angular speeds, and sway speeds are considered

available for feedback to the control system. However, the measurement vector is corrupted by the noise vector $\boldsymbol{\eta} = [\eta_1\ \eta_2\ \eta_3\ \eta_4\ \eta_5]$. Such measurement noise arises to any practical control system due to non-ideal sensors and instrumentation. In order to make a conservative assumption, the noise vector consists of five mutually uncorrelated, scalar, white, Gaussian noise components. The covariance (PSD) for each one of them is considered to be 10% of the maximum value expected for the corresponding variable, in the open-loop system. These values are calculated using the expressions in Eq. (24) which result to the ones in Eq. (25). Note that the temporal derivative expressions, i.e., $\dot{\psi}_{w,}, \dot{\varphi}_{\boldsymbol{w},}$ are connected according to the following with the expressions in Eq. (25).

$$\dot{\psi}_w(s) = s\psi_w(s), \dot{\phi}_w(s) = s\phi_w(s) \tag{30}$$

Furthermore, the other input signals arising are the process (wave) disturbances. Indeed, as seen in Fig. 6, the wave disturbances $\boldsymbol{w}_\psi$ and $_\varphi$ participate in the system according to the following.

$$\left.\begin{aligned} w_\psi(s) &= \frac{2\zeta_w\omega_0\sigma_{w,\psi}s}{s^2 + 2\zeta_w\omega_0 s + \omega_0^2}\cdot w_{G,1} \\ w_\phi(s) &= \frac{2\zeta_w\omega_0\sigma_{w,\phi}s}{s^2 + 2\zeta_w\omega_0 s + \omega_0^2}\cdot w_{G,2} \end{aligned}\right\}\Leftrightarrow$$
$$\begin{bmatrix} w_\psi(s) \\ w_\phi(s) \end{bmatrix} = h_w(s)\begin{bmatrix} \sigma_{w,\psi} & 0 \\ 0 & \sigma_{w,\phi} \end{bmatrix}\begin{bmatrix} w_{G,1}(s) \\ w_{G,2}(s) \end{bmatrix} \tag{31}$$

It is reminded here, that the vector $w_G = \begin{bmatrix} w_{G,1} & w_{G,2} \end{bmatrix}^T$ consists of two scalar, mutually independent, white, Gaussian stochastic processes of zero mean and unity standard deviation. According to the analysis given in Section 2.2, the parameters $\sigma_{w,\psi}$ and $\sigma_{w,\varphi}$ are uncertain with ranges given below.

$$0 \le \sigma_{w,\psi}, \sigma_{w,\phi} \le S(\omega_0) \le 10.0,\ 0.3 \le \omega_0 \le 1.3 \tag{32}$$

On the other hand, ζ_w may be set to a constant value; a typical one is 0.1. A highly convenient approach is to use Eq. (11) and the first inequality in Eq. (32), in order to use $[S(\omega_0)]^{-1}$ as a scaling factor, taking advantage of the fact that $\|h_w(s)\|_\infty = 1$. This scaling factor normalizes the disturbance inputs in the same manner that the outputs are normalized by Eq. (25).

3.5 Partitioning of the Full Control Model

The general control problem according to the recent literature (Green and Limebeer 1995; Tempo and Blanchini 1996; Zhou et al. 1996) may be posed on the basis of linear fractional transformations (LFTs). Linear fractional transformations have been introduced in order to represent any type of uncertainty arising in Single-Input, Single-Output (SISO) or MIMO linear systems, including multiplicative, additive, or feedback uncertainties. Moreover, apart from uncertainties, the LFT can be used for representing and analyzing elegantly the effect of feedback control. A brief reference to the robust stability and performance analysis in the LFT framework is given in Appendix 2.

The task here is to clearly establish the uncertain control model of Fig. 6 in an LFT framework as shown in Fig. 8. In this end, input vectors $\boldsymbol{u}_u$, $\boldsymbol{u}_0$, $\boldsymbol{u}_\ell$ and output vectors $\boldsymbol{y}_u$, $\boldsymbol{y}_0$, $\boldsymbol{y}_\ell$ need to be defined.

Starting from vectors $\boldsymbol{y}_u$ and $\boldsymbol{u}_u$ that enter and exit the uncertainty, respectively, we need to apply the procedure referred to as "pulling out the Δ's" in the literature (Zhou et al. 1996; Zhou and Doyle 1998; Tempo and Blanchini 1996; Skogestad and Postlethwaite 1996). Recalling which elements in the model of Fig. 7 are uncertain, the following consolidated matrix $\boldsymbol{\Delta}$ is obtained.

$$\boldsymbol{\Delta} = \begin{bmatrix} \Delta U\cdot\boldsymbol{A}_U & 0 & 0 & 0 \\ 0 & \Delta U\cdot\boldsymbol{B}_U & 0 & 0 \\ 0 & 0 & \Delta U\cdot\boldsymbol{\Phi}_U & 0 \\ 0 & 0 & 0 & \delta k_R \end{bmatrix} \tag{33}$$

Matrix with real-valued entries, this matrix is not square. Furthermore, in accordance with the $\boldsymbol{\Delta}$ defined above the following $\boldsymbol{y}_u$ and consequently $\boldsymbol{u}_u$ are defined.

$$\boldsymbol{y}_u = \begin{bmatrix} \boldsymbol{x} \\ \delta_R \\ \boldsymbol{w} \\ \delta_r \end{bmatrix}, \boldsymbol{u}_u = \boldsymbol{\Delta}\cdot\boldsymbol{y}_u \Rightarrow \boldsymbol{u}_u = \begin{bmatrix} \Delta U\cdot\boldsymbol{A}_U & 0 & 0 & 0 \\ 0 & \Delta U\cdot\boldsymbol{B}_U & 0 & 0 \\ 0 & 0 & \Delta U\cdot\boldsymbol{\Phi}_U & 0 \\ 0 & 0 & 0 & \delta k_R \end{bmatrix}\cdot\begin{bmatrix} \boldsymbol{x} \\ \delta_R \\ \boldsymbol{w} \\ \delta_r \end{bmatrix} \tag{34}$$

The second pair of vectors that will be constituted is $\boldsymbol{y}_\ell$ and $\boldsymbol{u}_\ell$ that enter and exit the controller, respectively. As explained in Section 3.4, the following inputs and outputs are associated with the RRS controller.

$$\boldsymbol{y}_\ell = \boldsymbol{C}\cdot\boldsymbol{x} + \boldsymbol{\eta} = \begin{bmatrix} r \\ \psi \\ p \\ \phi \end{bmatrix} + \begin{bmatrix} \eta_1 \\ \eta_2 \\ \eta_3 \\ \eta_4 \end{bmatrix}, \boldsymbol{u}_\ell = \delta_{\text{set}} \tag{35}$$

In order to partition the process block to the nine subblocks, as indicated in Eq. (B.1) and Fig. 8, the following input and output vectors $\boldsymbol{u}_0$ and $\boldsymbol{y}_0$ respectively are defined.

$$\boldsymbol{y}_0 = \begin{bmatrix} \boldsymbol{C}_0\cdot\boldsymbol{x} \\ H_{\text{steer},0}(s)\cdot\delta_{\text{set}} \end{bmatrix} = \begin{bmatrix} 0.1904\cdot\psi \\ 0.1476\cdot\phi \\ H_{\text{steer},0}(s)\cdot\delta_{\text{set}} \end{bmatrix}, \boldsymbol{u}_0 = \begin{bmatrix} \boldsymbol{w} \\ \boldsymbol{\eta} \end{bmatrix} \tag{36}$$

Vector $\boldsymbol{w} = \begin{bmatrix} w_\psi & w_\phi \end{bmatrix}^{\mathrm{T}}$ is the exogenous disturbance vector appearing in Eq. (3) and the vector $\boldsymbol{\eta}$ is the measurement noise vector appearing in Fig. 6 consisting of two scalar, mutually

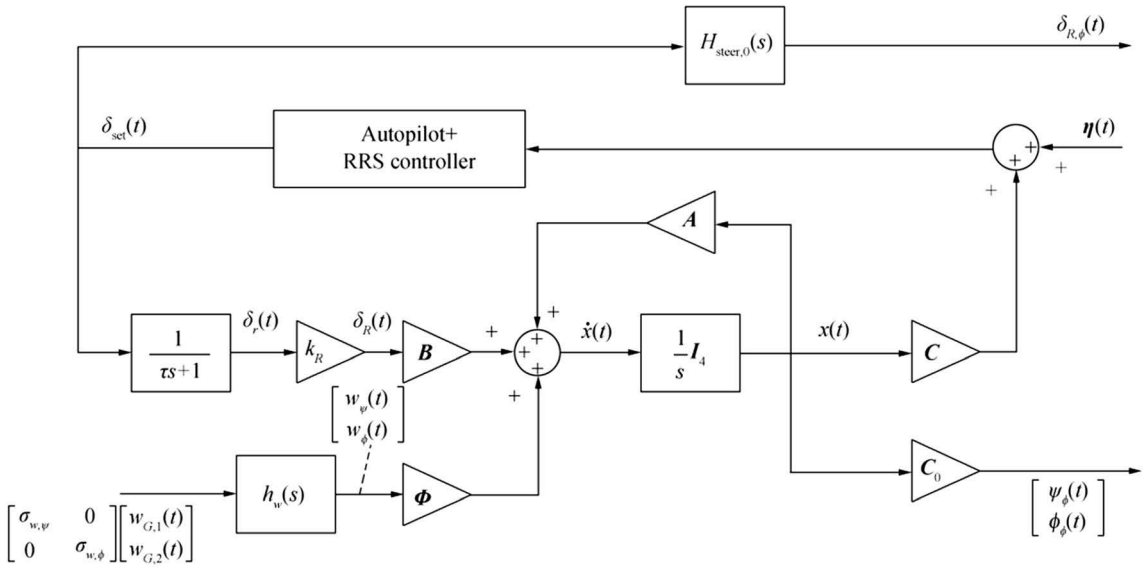

Fig. 7 Full control system model of naval vessel with autopilot and RRS system

independent, white, Gaussian stochastic processes of zero mean and unity standard deviation. By employing the above definitions, the following sub-blocks of the process block $\boldsymbol{P}$ may be defined.

$$\boldsymbol{P}_{11} = \begin{bmatrix} (s\boldsymbol{I}_5-\boldsymbol{A}_0)^{-1} & (s\boldsymbol{I}_5-\boldsymbol{A}_0)^{-1} & \boldsymbol{0}_{1\times5} & (s\boldsymbol{I}_5-\boldsymbol{A}_0)^{-1} & (s\boldsymbol{I}_5-\boldsymbol{A}_0)^{-1}\boldsymbol{B}_0 & 1 \\ \boldsymbol{0}_{1\times5} & & \boldsymbol{0}_{2\times5} & \boldsymbol{0}_{1\times5} & & \boldsymbol{0}_{2\times1} \\ \boldsymbol{0}_{2\times5} & & \boldsymbol{0}_{1\times5} & \boldsymbol{0}_{2\times5} & & 0 \\ \boldsymbol{0}_{1\times5} & & & \boldsymbol{0}_{1\times5} & & \end{bmatrix}$$

$$\boldsymbol{P}_{12} = \begin{bmatrix} (s\boldsymbol{I}_5-\boldsymbol{A}_0)^{-1}\boldsymbol{\Phi}_0 & \boldsymbol{0}_{5\times4} \\ \boldsymbol{0}_{1\times2} & \boldsymbol{0}_{1\times4} \\ \boldsymbol{I}_2 & \boldsymbol{0}_{2\times4} \\ \boldsymbol{0}_{1\times2} & \boldsymbol{0}_{1\times4} \end{bmatrix}$$

$$\boldsymbol{P}_{13} = \begin{bmatrix} (s\boldsymbol{I}_5-\boldsymbol{A}_0)^{-1}\boldsymbol{B}_0 k_{R0}H(s) \\ k_{R0}H(s) \\ \boldsymbol{0}_{2\times1} \\ H(s) \end{bmatrix} \tag{37}$$

$$\boldsymbol{P}_{21} = \begin{bmatrix} \boldsymbol{C}_0(s\boldsymbol{I}_5-\boldsymbol{A}_0)^{-1} & \boldsymbol{C}_0(s\boldsymbol{I}_5-\boldsymbol{A}_0)^{-1} & \boldsymbol{C}_0(s\boldsymbol{I}_5-\boldsymbol{A}_0)^{-1} & \boldsymbol{C}_0(s\boldsymbol{I}_5-\boldsymbol{A}_0)^{-1}\boldsymbol{B}_0 \\ \boldsymbol{0}_{1\times5} & \boldsymbol{0}_{1\times5} & \boldsymbol{0}_{1\times5} & 0 \end{bmatrix}$$

$$\boldsymbol{P}_{22} = \begin{bmatrix} \boldsymbol{C}_0(s\boldsymbol{I}_5-\boldsymbol{A}_0)^{-1}\boldsymbol{\Phi}_0 & \boldsymbol{0}_{2\times4} \\ \boldsymbol{0}_{1\times2} & \boldsymbol{0}_{1\times4} \end{bmatrix}$$

$$\boldsymbol{P}_{23} = \begin{bmatrix} \boldsymbol{C}_0(s\boldsymbol{I}_5-\boldsymbol{A}_0)^{-1}\boldsymbol{B}_0 k_{R0}H(s) \\ H_{\text{steer},0}(s) \end{bmatrix} \tag{38}$$

$$\boldsymbol{P}_{31} = \begin{bmatrix} \boldsymbol{C}(s\boldsymbol{I}_5-\boldsymbol{A}_0)^{-1} & \boldsymbol{C}(s\boldsymbol{I}_5-\boldsymbol{A}_0)^{-1}\boldsymbol{C}(s\boldsymbol{I}_5-\boldsymbol{A}_0)^{-1} & \boldsymbol{C}(s\boldsymbol{I}_5-\boldsymbol{A}_0)^{-1}\boldsymbol{B}_0 \end{bmatrix}$$

$$\boldsymbol{P}_{32} = \begin{bmatrix} \boldsymbol{C}(s\boldsymbol{I}_5-\boldsymbol{A}_0)^{-1}\boldsymbol{\Phi}_0 & \boldsymbol{I}_4 \end{bmatrix} \tag{39}$$

$$\boldsymbol{P}_{33} = \begin{bmatrix} \boldsymbol{C}(s\boldsymbol{I}_5-\boldsymbol{A}_0)^{-1}\boldsymbol{B}_0 k_{R0}H(s) \end{bmatrix}$$

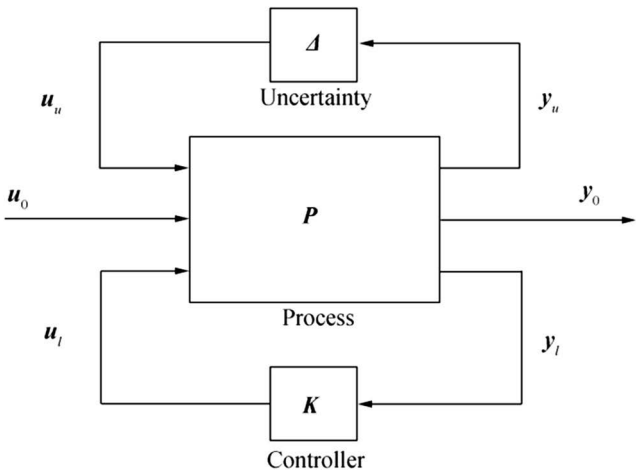

Fig. 8 The linear fractional transformation framework

4 Frigate RRS Robust Controller Synthesis and Validation

4.1 Synthesis of the RRS Suboptimal H_∞ Robust Controller

In the majority of the cases where a naval vessel might need roll stabilization support, the ship speed is high or equal to the nominal value of 15 kn assumed in Section 3.1. Therefore, a good practice would be to design an RRS system controller for this speed value by neglecting the uncertainty. After a controller is obtained, by employing the LFT framework as in the well well-known study (Doyle et al. 1989), the uncertainty is re-attached in order to investigate the robustness of the closed-loop system.

As has been shown in Appendix 2, if the uncertainty $\boldsymbol{\Delta}$ is identically zero in Fig. 8, then Eq. (B.4) holds. Synthesis aims to design the controller $K(s)$ so that an H_∞-norm objective is

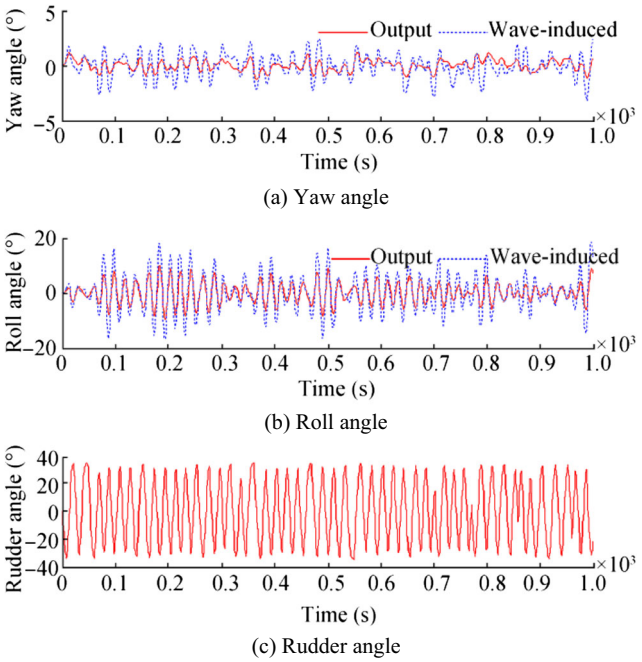

Fig. 9 Control performances of the autopilot with RRS based on compact H_∞ design

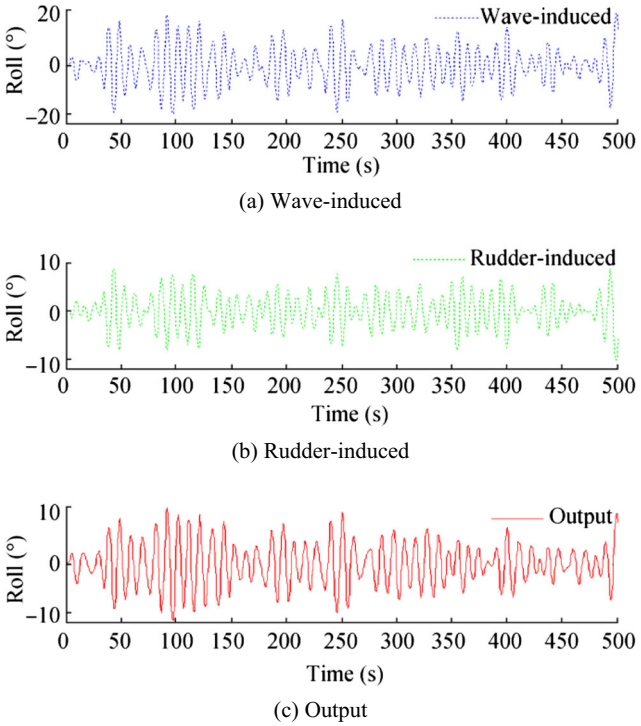

Fig. 10 Roll angles comparison of the autopilot with RRS based on compact H_∞ design

met. However, as the H_∞ norm is the $\boldsymbol{L}_2$ to $\boldsymbol{L}_2$-induced norm of $\boldsymbol{G} = \boldsymbol{F}_\ell(\boldsymbol{P}, \boldsymbol{K})$, if this norm is minimized, then the worst case energy of response signal vector y_0 over all bounded energy excitation signal vectors u_0 is minimized as well.

Denote as $\gamma(\boldsymbol{K})$, the closed-loop value achieved a particular controller $\boldsymbol{K}$, i.e., $\gamma(\boldsymbol{K}) = \|\boldsymbol{F}_\ell(\boldsymbol{P}, \boldsymbol{K})\|_\infty$. It can be expected that a specific choice of a stable controller, maintaining the stability of the closed-loop, minimizes $\gamma(\boldsymbol{K})$. This stable and stabilizing controller is denoted as $\boldsymbol{K}_{\text{opt}}$ and the achieved value of $\gamma(\boldsymbol{K})$ as γ_{opt}. However, in our RRS controller design problem, γ_{opt} is not known a priori. Therefore, the calculation procedure of $\boldsymbol{K}_{\text{opt}}$ involves some form of optimization. In Doyle et al. (1989) and Glover and Doyle (1988), the optimization is implemented through a numerical, iterative technique, which leads to a value of close to γ_{opt}, but not to γ_{opt}, exactly.

In our case, the controller calculation procedure involves the selection of an initial guesstimate for γ. For this value, the following Hamiltonian matrices are used. Note that the partitioning of the process plant matrices given in Section 3.5 is used.

$$\boldsymbol{H}_\infty \triangleq \begin{bmatrix} \boldsymbol{A} & \gamma^{-2}\boldsymbol{B}_1\boldsymbol{B}_1^{\mathrm{T}} - \boldsymbol{B}_2\boldsymbol{B}_2^{\mathrm{T}} \\ -\boldsymbol{C}_1^{\mathrm{T}}\boldsymbol{C}_1 & -\boldsymbol{A}^{\mathrm{T}} \end{bmatrix}$$
$$\boldsymbol{J}_\infty \triangleq \begin{bmatrix} \boldsymbol{A}^{\mathrm{T}} & \gamma^{-2}\boldsymbol{C}_1^{\mathrm{T}}\boldsymbol{C}_1 - \boldsymbol{C}_2^{\mathrm{T}}\boldsymbol{C}_2 \\ -\boldsymbol{B}_1\boldsymbol{B}_1^{\mathrm{T}} & -\boldsymbol{A} \end{bmatrix} \tag{40}$$

Having formulated $\boldsymbol{H}_\infty$, $\boldsymbol{J}_\infty$, the following conditions are checked: (a) $\boldsymbol{H}_\infty$, $\boldsymbol{J}_\infty$ must not obtain purely imaginary eigenvalues. (b) The stabilizing solutions of the Algebraic Riccati Equations, associated with the Hamiltonian matrices $\boldsymbol{H}_\infty$, $\boldsymbol{J}_\infty$, denoted as $\boldsymbol{X}_\infty = \mathrm{Ric}(\boldsymbol{H}_\infty)$, $\boldsymbol{Y}_\infty = \mathrm{Ric}(\boldsymbol{J}_\infty)$ are positive, semidefinite matrices (Doyle et al. 1989; Glover and Doyle 1988). (c) The spectral radius $\rho(\boldsymbol{X}_\infty\boldsymbol{Y}_\infty) < \gamma^2$. If these conditions are met, then a stable and stabilizing controller, $\boldsymbol{K}_\infty$, may be calculated using the calculated matrices $\boldsymbol{H}_\infty$, $\boldsymbol{J}_\infty$, $\boldsymbol{X}_\infty$, $\boldsymbol{Y}_\infty$. The controller obtained achieves $\|\boldsymbol{G}(s)\|_\infty = \|\boldsymbol{F}_\ell(\boldsymbol{P}, \boldsymbol{K})\|_\infty \le \gamma$. If this value of γ is not satisfactory, then it is reduced and the procedure is iterated until stopped either because the obtained value of $\gamma = \hat{\gamma}$ is satisfactorily small or because one of the conditions is not met. The controller obtained in this manner, $\boldsymbol{K}_\infty$, is referred to as suboptimal $\boldsymbol{H}_\infty$ controller, as it achieves a value of γ generally larger than γ_{opt}.

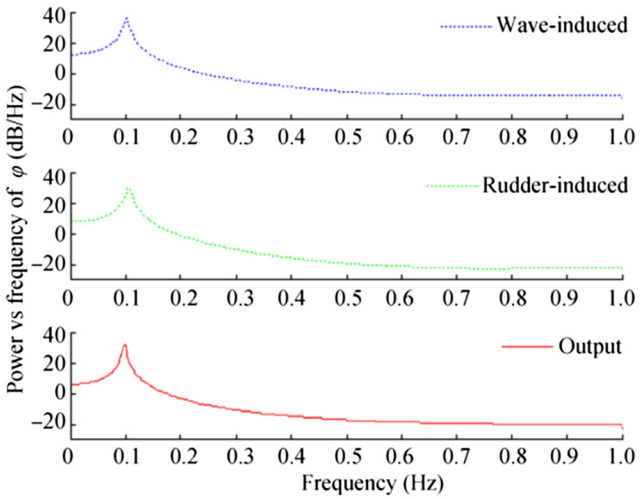

Fig. 11 Power spectral density estimate via Yule-Walker of roll angles

Table 1 Performance of H_2 and H_∞ controllers at $U = 5$ kn

Performances		$\Re$ %	ψ (°)	δ (°)
SISO	H_2	45.4	0.42	20.8
	H_∞	45.4	0.79	21.1
MIMO	H_2	45.5	0.32	20.3
	H_∞	47.4	0.45	20.8

Note that the describing function of the saturation nonlinearity, defined above, for zero bias sinusoidal excitation is purely real. An alternative expression for $N_{\text{sat}}(A_\delta, 0)$ is given below.

$$N_{\text{sat}}(A_\delta,0)=\begin{cases}\gamma, |A_\delta|<\rho\\ \dfrac{2\gamma}{\pi}[\psi+cos(\psi)\sin(\psi)], \psi\triangleq\arcsin\left(\dfrac{\rho}{A_\delta}\right), |A_\delta|>\rho\end{cases} \tag{41}$$

5 H_2 Linear Quadratic Gaussian Regulator for Rudder Roll Stabilization

The linear quadratic Gaussian (LQG) control problem for a stochastic system like the vessel in this work undergoing roll motion due to exogenous disturbances is historically the most prominent and basic optimal control problem (Zhou and Doyle 1998; Skogestad and Postlethwaite 1996; Martin 1985). The problem setup concerns a linear, time-invariant system where both the process disturbance and the measurement noise are modeled as Gaussian white noise stochastic signals, uncorrelated between themselves and to other inputs to the system.

$$\begin{aligned}\dot{\boldsymbol{x}}&=\boldsymbol{A}\boldsymbol{x}+\boldsymbol{B}\boldsymbol{u}+\boldsymbol{d}\\ \boldsymbol{y}&=\boldsymbol{C}\boldsymbol{x}+\boldsymbol{\eta}\end{aligned} \tag{42}$$

The process disturbance $\boldsymbol{d}$ as well as the measurement noise $\boldsymbol{\eta}$ above are both white and Gaussian with covariance matrix $\boldsymbol{W}$ and $\boldsymbol{V}$, respectively (Zhou and Doyle 1998; Skogestad and Postlethwaite 1996). However, no uncertainty is accounted for. In the context of a rolling vessel, vectors $\boldsymbol{x}$, $\boldsymbol{u}$, $\boldsymbol{y}$, $\boldsymbol{d}$, and $\boldsymbol{\eta}$ as well as matrices $\boldsymbol{A}$, $\boldsymbol{B}$, and $\boldsymbol{C}$ have been defined before and will not be repeated here in the interest of brevity. The standard LQG problem is to find a control signal $u(t)$ so that the cost function defined hereafter is minimized.

$$J_{\text{LQG}}=E\left\{\lim_{T\to\infty}\frac{1}{T}\int_0^T\left(\boldsymbol{x}^{\text{T}}\boldsymbol{Q}\boldsymbol{x}+\boldsymbol{u}^{\text{T}}\boldsymbol{R}\boldsymbol{u}\right)\mathrm{d}t\right\} \tag{43}$$

Table 2 Performance of H_2 and H_∞ controllers at $U = 10$ kn

Performances		$\Re$ %	ψ (°)	δ (°)
SISO	H_2	52.4	0.48	20.6
	H_∞	45.8	0.55	20.9
MIMO	H_2	51.3	0.29	19.3
	H_∞	48.1	0.40	21.1

Table 3 Performance of H_2 and H_∞ controllers at $U = 15$ kn

Performances		$\Re$ %	ψ (°)	δ (°)
SISO	H_2	57.7	0.38	19.3
	H_∞	38.7	0.58	20.3
MIMO	H_2	48.5	0.41	19.3
	H_∞	44.8	0.49	21.3

In the above, $\boldsymbol{Q}$ and $\boldsymbol{R}$ are appropriate real, symmetric, positive-definite matrices holding design parameter or weighing values.

This problem can be solved by a full state feedback control law of the form (Zhou and Doyle 1998; Skogestad and Postlethwaite 1996):

$$\boldsymbol{u}=-\boldsymbol{K}_s\boldsymbol{x}, \boldsymbol{K}_s=\boldsymbol{R}^{-1}\boldsymbol{B}^{\text{T}}\boldsymbol{X} \tag{44}$$

Matrix $\boldsymbol{X}$ is determined as the unique symmetric real positive-semidefinite solution of the following algebraic Riccati equation (Zhou and Doyle 1998; Skogestad and Postlethwaite 1996):

$$\boldsymbol{A}^{\text{T}}\boldsymbol{X}+\boldsymbol{X}\boldsymbol{A}-\boldsymbol{X}\boldsymbol{B}\boldsymbol{R}^{-1}\boldsymbol{B}^{\text{T}}\boldsymbol{X}+\boldsymbol{Q}=0 \tag{45}$$

In case that the full state vector is not available for feedback, a Kalman filter can be employed to generate an estimate for the state vector that can be used instead (Zhou and Doyle 1998; Skogestad and Postlethwaite 1996). The Kalman filter obtains the familiar form of a state observer.

$$\dot{\hat{\chi}}=A\hat{\chi}+K_f\left(y-C\hat{\chi}\right) \tag{46}$$

In the above, "hat" implies estimate. $\boldsymbol{K}_f$ is chosen so that the expectation value of the state error vector as follows is minimum.

$$\min E\left\{(\chi-\hat{\chi})^{\text{T}}(\chi-\hat{\chi})\right\} \tag{47}$$

The value of $\boldsymbol{K}_f$ that achieves minimum state square error is proven to be the following.

$$\boldsymbol{K}_f=\boldsymbol{Y}\boldsymbol{C}^{\text{T}}\boldsymbol{V}^{-1} \tag{48}$$

Matrix $\boldsymbol{Y}$ above is the unique symmetric real positive-semidefinite solution of the following algebraic Riccati equation (Zhou and Doyle 1998; Skogestad and Postlethwaite 1996):

Table 4 Performance of H_2 and H_∞ controllers at $U = 20$ kn

Performances		$\Re$ %	ψ (°)	δ (°)
SISO	H_2	55.5	0.44	18.8
	H_∞	31.9	0.55	20.0
MIMO	H_2	42.7	0.47	19.2
	H_∞	39.6	0.56	22.0

Table 5 Performance of H_2 and H_∞ controllers at $U = 25$ kn

Performances		$\Re$ %	ψ (°)	δ (°)
SISO	H_2	48.8	0.51	18.9
	H_∞	38.8	0.98	25.5
MIMO	H_2	36.2	0.51	19.2
	H_∞	37.2	0.57	22.1

$$\boldsymbol{Y}\boldsymbol{A}^{\mathrm{T}} + \boldsymbol{A}\boldsymbol{Y} - \boldsymbol{Y}\boldsymbol{C}^{\mathrm{T}}\boldsymbol{V}^{-1}\boldsymbol{C}\boldsymbol{Y} + \boldsymbol{W} = 0 \tag{49}$$

As a concluding remark, we mention that the LQG problem presented here can be put in the more general framework of H_2 control synthesis where the standard optimal control problem is to find a stabilizing controller $\boldsymbol{K}$ so that the H_2 norm of the following LFT is minimized.

$$\|\boldsymbol{F}(s)\|_2 = \sqrt{\frac{1}{2\pi}\int_{-\infty}^{+\infty} \boldsymbol{F}(mathrmj\omega)\boldsymbol{F}^{\mathrm{T}}(\mathrm{j}\omega)\mathrm{d}\omega}, \quad \boldsymbol{F} \triangleq \boldsymbol{F}_\ell(\boldsymbol{P}, \boldsymbol{K}) \tag{50}$$

The generalized plant $\boldsymbol{P}$ in the above is appropriately defined in order to incorporate the original system dynamics as well as covariance matrices $\boldsymbol{W}$ and $\boldsymbol{V}$ and weighing matrices $\boldsymbol{R}$ and $\boldsymbol{Q}$ introduced earlier (Zhou and Doyle 1998; Skogestad and Postlethwaite 1996). The generalized plant's structure and form resembles closely that for H_∞ controller synthesis.

6 Numerical Simulation

6.1 Simulation Configuration

The nominal test is done for water speed 15 kn. The wave encountering period is set to 10 s, that is 0.63 rad/s in frequency, the standard deviation of the wave-induced roll is 6.65° with a max roll angle 20°, the standard deviation of the wave-induced yaw is 1.05° with a max course error 3°, the rudder angle of deviation $|\delta_{\mathrm{set}}(t)|$ and its turning rate $|\dot{\delta}_R(t)|$ are no greater than 35° and 15°/s. Since the linearized vessel model is employed, the set course (reference value) is 0 in the simulation runs. The wave encounter frequency is defined in Eq. (12) in Section 2.2 as well as in Eq. (26) in Section 3.2.

Table 6 Performance of H_2 and H_∞ controllers at $\omega_0 = 0.3$rad/s, $\phi_{\mathrm{wave}} = 6.7$, $\psi_{\mathrm{wave}} = 4.4$

Performances		$\Re$ %	ψ (°)	δ (°)
SISO	H_2	60.7	1.64	23.2
	H_∞	58.2	1.74	25.2
MIMO	H_2	64.2	1.40	25.5
	H_∞	54.7	1.94	27.5

Table 7 Performance of H_2 and H_∞ controllers at $\omega_0 = 0.5$rad/s, $\phi_{\mathrm{wave}} = 7.4$, $\psi_{\mathrm{wave}} = 1.9$

Performances		$\Re$ %	ψ (°)	δ (°)
SISO	H_2	61.8	0.58	20.5
	H_∞	48.8	0.71	21.4
MIMO	H_2	58.3	0.58	20.8
	H_∞	46.4	0.74	22.8

6.2 Simulation Results

The simulation results of the proposed H_∞ controller applied to a vessel in a seaway are shown in Figs. 9, 10, and 11. As can be seen, the H_∞ control system achieves good performance of joint course keeping and RRS. In the nominal simulation test of the compact H_∞ design, the wave-induced yaw disturbance has been attenuated by 53.9% without any steady steady-state error. At the same time, the RRS effect is remarkable with a damping ratio of 48.5%. Such control performance is more prominent when the upper high-frequency input of the rudder angle is greatly increased as shown in Fig. 9.

Figures 10 and 11 demonstrate the operating principle of rudder roll stabilization. Specifically, the non-zero-mean, low-frequency, aperiodic activity to maintain heading and course of the vessel is augmented by superposition of a high-frequency, zero-mean periodic steering to counter roll motion. Furthermore, as clearly seen in Fig. 10, the instantaneous roll angle induced by the waves and the one induced by the rudder activity are clearly of opposite phase. The same conclusion is also supported by the frequency domain (Fourier) analysis shown in Fig. 11.

Tables 1, 2, 3, 4, and 5 show the comparative performance of the proposed controllers at different ship speeds. It is evident that all four robust control designs exhibit excellent robustness in the face of the model perturbation caused by speed variation. In general, H_2 controllers employ significant less rudder activity to achieve better anti-rolling rate and smaller course error as compared with H_∞ controllers in both the SISO and MIMO design. As speed increases, control performance improves first and then decreases.

Control performance of the H_2 controller (SISO) demonstrates the typical normal distribution patterns with the optimum occurring in the vicinity of speed of 15 kn. The optimal control performance for the other three controllers (Tables 6,

Table 8 Performance of H_2 and H_∞ controllers at $\omega_0 = 0.7$rad/s, $\phi_{\mathrm{wave}} = 5.8$, $\psi_{\mathrm{wave}} = 0.9$

Performances		$\Re$ %	ψ (°)	δ (°)
SISO	H_2	55.7	0.35	18.4
	H_∞	38.9	0.48	19.7
MIMO	H_2	46.0	0.36	18.6
	H_∞	48.7	0.49	21.2

Table 9 Performance of H_2 and H_∞ controllers at $\omega_0 = 0.9$rad/s, $\phi_{\text{wave}} = 3.0$, $\psi_{\text{wave}} = 0.5$

Performances		$\Re$ %	ψ (°)	δ (°)
SISO	H_2	58.1	0.26	17.0
	H_∞	33.2	0.37	19.2
MIMO	H_2	48.6	0.26	17.1
	H_∞	49.2	0.41	21.2

7, and 8) appears at speed around 10 kn; also, note that control performance at low speed is better than that at high speed.

As can be seen in Table 2, in the wave frequency domain, the roll response due to wave disturbance is greatest about the natural rolling frequency of the ship, while the wave-induced yaw decreases with increase in frequency. The H_2 controller achieves better anti-rolling rates over the whole frequency domain. The H_2 SISO design achieves in average 6.9% higher than that of the MIMO design. A similar behavior is also observed for course control. Compared with the H_2 designs, H_∞ controllers perform slightly worse with higher rudder activity. H_∞controllers perform better at lower frequencies than at higher ones (Table 9). It is worth noting that H_∞ controllers configured by SISO design fail to attenuate the wave-induced disturbances when the wave frequency is higher than 1.1 rad/s (Table 10), although the high-frequency response is relatively small. Furthermore, MIMO H_∞ controllers work better than SISO ones, but they have similar shortcomings at the frequency of 1.3 rad/s (Table 11). In brief, H_2 control design shows good robustness and effectiveness over the whole wave frequency domain while H_∞ cannot achieve the same in the high-frequency range.

In order to verify the robustness of the control system and the performance under different interference conditions, two sets of comparative experiments were conducted. Firstly, comparative tests are done with the ship speeds ranging from 5 to 25 kn, which is to detect the robustness and effectiveness of the proposed control system in the case of model perturbations caused by velocity changing; secondly, the effectiveness of the control system is tested in the full wave frequency domain ranging from 0.3 to 1.3 rad/s, with ship speed is set to 15 kn. The roll reduction rate is defined as follows

$$\Re\% = \frac{w_\varphi - \Phi_{\text{RRS}}}{w_\varphi} \tag{51}$$

where w_φ is the STD value of wave-induced roll and Φ_{RRS} is the STD value of roll with RRS control.

Table 10 Performance of H_2 and H_∞ controllers at $\omega_0 = 1.1$rad/s, $\phi_{\text{wave}} = 1.6$, $\psi_{\text{wave}} = 0.3$

Performances		$\Re$ %	ψ (°)	δ (°)
SISO	H_2	60.1	0.21	15.4
	H_∞	0.5	0.36	20.0
MIMO	H_2	48.6	0.20	15.7
	H_∞	32.5	0.36	23.1

Table 11 Performance of H_2 and H_∞ controllers at $\omega_0 = 1.3$rad/s, $\phi_{\text{wave}} = 1.0$, $\psi_{\text{wave}} = 0.2$

Performances		$\Re$ %	ψ (°)	δ (°)
SISO	H_2	62.9	0.14	13.4
	H_∞	− 52.9	0.35	20.0
MIMO	H_2	52.2	0.13	13.6
	H_∞	1.2	0.29	23.4

It is worth noting that, because the sea state interference is driven by random white noise, the experimental results are of some randomness, but the accuracy and physical significance are not affected.

7 Conclusions

This paper investigates the effectiveness of augmenting the rudder use for rejecting part of the unwanted roll, while maintaining steering and course changing ability. Specifically, an anti-rolling action is enabled through intentional superposition of fast, high-frequency rudder activity as compared with rudder movement to implement course change and keeping.

The high-frequency movements of the rudder are in the frequency range of the roll excitation due to exogenous environmental wave disturbances. In effect, this superimposed rudder activity attenuates the high-frequency roll effects from encountering rough seas when appropriately tuned. For this purpose, H_∞ and H_2 robust controllers are designed. To test and evaluate those controllers, an appropriate control model of the ship dynamics and the steering gear which is the critical piece of actuator equipment allowing this technique to be used is implemented. Random wave disturbances and noise components are applied to the model; to generate them the stochastic processes involved are properly modeled and validated.

The results presented concern a fast naval combat ship, specifically a displacement frigate vessel. However, with appropriate modifications, this technique can be applied to other displacement hull types. With further modifications and analysis, it can be adapted to entirely different vessel types like planing craft and hydrofoil boats. The only fundamental prerequisite is the use of a single or multiple conventional rudders for steering rather than, e.g., waterjets or pods. These applications will be investigated in future works.

Appendix 1: Describing Functions of SISO Nonlinearities

The describing function is a very useful tool for the analysis of SISO nonlinear systems, especially in the case of limit cycle oscillations. Therefore, they may be of value for the analysis

and synthesis of control loops involving actuating elements with nonlinear behavior. This behavior is quite unrestricted in form; e.g., it may be multi-valued and/or discontinuous and soft or hard. In the sequel, the following input-output representation of a causal SISO nonlinear dynamic system is considered.

$$y(t) = f(x(\xi; -\infty < \xi \le t)) \tag{A.1}$$

In the above, $x(t)$ is the input or excitation signal and $y(t)$ is the output or response signal of the nonlinear system. Functional $f(\bullet)$ is the nonlinear input-output relationship of the system. The class of input signals to be considered will be of the following form.

$$x(t) = a_0 + a_1\cos(\omega t) = a_0 + \mathrm{Re}\{a_1 e^{j\omega t}\} \tag{A.2}$$

Therefore, the triad $(\omega, \alpha_1, \alpha_0)$ fully defines the input waveform in our context. In this case, an approximation the output signal obtains the following form.

$$y(t) \simeq b_0 + b_1\cos(\omega t + \phi) = b_0 + \mathrm{Re}\{b_1 e^{j\phi} e^{j\omega t}\} \tag{A.3}$$

In this respect, the describing function is defined as the following complex number.

$$N(\omega, a_1, a_0) = \frac{b_1}{a_1} e^{j\phi} \tag{A.4}$$

The most common approximation criterion is the mean square error (MSE) over one fundamental period of the input. A rather useful manner to obtain $N(\omega, \alpha_1, \alpha_0)$ analytically is by minimization of the MSE.

$$J_2 = \int_0^{\frac{2\pi}{\omega}} \left[f(a_0 + a_1\cos\omega t) - b_0 - \mathrm{Re}\{a_1 N(\omega, a_1, a_0) e^{j\omega t}\}\right]^2 dt \tag{A.5}$$

In our context, it can be shown that b_0 and $[a_1 N(\omega, a_1, a_0)]$ are the constant (DC) bias and first harmonic coefficients, respectively, of the Fourier expansion of the output waveform $f(a_0 + a_1 \cos \omega t)$ (Nagrath and Gopal 1986; Zhou 1987). Note that this approximation of a nonlinear characteristic actually retains two important properties: amplitude dependence and the coupling between the DC bias and fundamental harmonic terms. The latter property is a result of the fact that superposition does not hold for nonlinear systems; thus, the describing function, $N(\omega, a_1, a_0)$, is a transfer function parameterized by input signal amplitude (i.e., function of a_1) and operating point (i.e., function of the bias a_0).

Although in related literature (Nagrath and Gopal 1986; Zhou 1987), $f(\bullet)$ may assume much more general forms, for the purpose of steering gear modeling of a system consisted of a static nonlinearity $M(\bullet)$ followed by a low-pass transfer function $G(\omega)$ will be considered, as depicted in Fig. 3. It can be seen that the describing function of a static memoryless nonlinearity is not frequency dependent. In effect, for the nonlinear system in Fig. 3, the following holds.

$$N(\omega, a_1, a_0) = N_M(a_1, a_0) G(\omega) \tag{A.6}$$

In the above, N_M (α_1, α_0) is the frequency independent describing function of the standalone memoryless nonlinearity $M(\bullet)$. In the case of the saturation nonlinearity for zero bias sinusoidal excitation, the describing function is given below.

$$M_{\mathrm{sat}}(x) = \begin{cases} -\mu, x < -\rho \\ \gamma x, |x| \le \rho, \mu \triangleq \rho\gamma \Rightarrow N_{\mathrm{sat}}(A,0) = \gamma\left\{\frac{2}{\pi}\left[\arcsin(\xi) + \xi\sqrt{1-\xi^2}, |\xi| \le 1\right]\right\} + j0 \\ +\mu, x < +\rho \end{cases} \begin{matrix} \\ \pm 1, |\xi| > 1, \rho \triangleq A\xi \\ \\ \end{matrix} \tag{A.7}$$

Note that the describing function of the saturation nonlinearity, defined above, for zero bias sinusoidal excitation is purely real. An alternative expression for N_{sat} $(A_c, 0)$ is given below.

$$\boldsymbol{N}_{\mathrm{sat}}(\boldsymbol{A_c}, 0) = \begin{cases} \gamma, |\boldsymbol{A}_c| < \rho \\ \frac{2\gamma}{\pi}[\psi + \cos(\psi)\sin(\psi)], \psi \triangleq \arcsin\left(\frac{\rho}{A_c}\right), |A_c| > \rho \end{cases}$$

$$\boldsymbol{K_N} = \begin{cases} \boldsymbol{K}, & \forall \boldsymbol{X} < s \\ \boldsymbol{K}\frac{2}{\pi}(\beta + \sin(\beta) \times \cos(\beta)), & \forall \boldsymbol{X} < s \end{cases} \tag{A.8}$$

Appendix 2: Robust Stability and Performance of Linear Systems

The generic framework for the representation of a MIMO uncertain linear system with feedback control is given in Fig. 8. The following partitioning of the process matrix $\boldsymbol{P}$ is considered.

$$\begin{bmatrix} \boldsymbol{y}_u \\ \boldsymbol{y}_0 \\ \boldsymbol{y}_\ell \end{bmatrix} = \begin{bmatrix} \boldsymbol{P}_{11} & \boldsymbol{P}_{12} & \boldsymbol{P}_{11} \\ \boldsymbol{P}_{21} & \boldsymbol{P}_{22} & \boldsymbol{P}_{23} \\ \boldsymbol{P}_{31} & \boldsymbol{P}_{32} & \boldsymbol{P}_{33} \end{bmatrix} \begin{bmatrix} \boldsymbol{u}_u \\ \boldsymbol{u}_0 \\ \boldsymbol{u}_\ell \end{bmatrix} \tag{B.1}$$

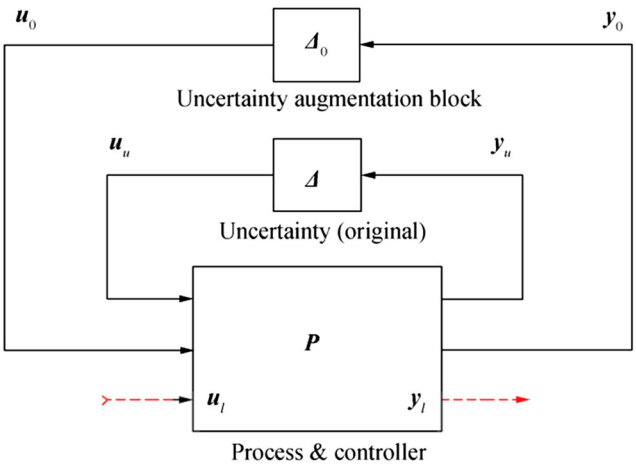

Fig. B1 The linear fractional transformation setup for checking robust performance

Furthermore, the following hold.

$$\boldsymbol{u}_u = \boldsymbol{\Delta}\cdot\boldsymbol{y}_u, \boldsymbol{u}_\ell = \boldsymbol{K}\cdot\boldsymbol{y}_\ell \tag{B.2}$$

For the open-loop plant, i.e., $\boldsymbol{K} \equiv \boldsymbol{0} \Rightarrow \boldsymbol{u}_\ell, \boldsymbol{y}_\ell = 0$, the following input-output relationship is concluded.

$$\begin{aligned} &\boldsymbol{y}_0 = \left[\boldsymbol{P}_{21}\boldsymbol{\Delta}(\boldsymbol{I}-\boldsymbol{P}_{11}\boldsymbol{\Delta})^{-1}\boldsymbol{P}_{12} + \boldsymbol{P}_{22}\right]\cdot\boldsymbol{u}_0 \Longleftrightarrow \\ &\boldsymbol{y}_0 = \boldsymbol{F}_u(\boldsymbol{P}, \boldsymbol{\Delta})\cdot\boldsymbol{u}_0 \end{aligned} \tag{B.3}$$

In the above, $\boldsymbol{F}_u(\boldsymbol{P}, \boldsymbol{\Delta})$ stands for the upper LFT of process $\boldsymbol{P}$ by the uncertainty $\boldsymbol{\Delta}$. In the same manner, if $\boldsymbol{\Delta} \equiv \boldsymbol{0} \Rightarrow \boldsymbol{u}_u, \boldsymbol{y}_u = 0$, the lower LFT of process $\boldsymbol{P}$ by the controller $\boldsymbol{K}$ is obtained.

$$\begin{aligned} &\boldsymbol{y}_0 = \left[\boldsymbol{P}_{22}\boldsymbol{K}(\boldsymbol{I}-\boldsymbol{P}_{32}\boldsymbol{K})^{-1}\boldsymbol{P}_{33} + \boldsymbol{P}_{23}\right]\cdot\boldsymbol{u}_0 \\ &\boldsymbol{y}_0 = \boldsymbol{F}_\ell(\boldsymbol{P}, \boldsymbol{K})\cdot\boldsymbol{u}_0 \end{aligned} \tag{B.4}$$

Evidently, the following relationships hold in the general case where both a controller and uncertainty are present.

$$\boldsymbol{y}_0 = \boldsymbol{F}_\ell(\boldsymbol{F}_u(P, \boldsymbol{\Delta}), \boldsymbol{K})\cdot\boldsymbol{u}_0 = \boldsymbol{F}_u(\boldsymbol{F}_\ell(\boldsymbol{P}, \boldsymbol{K}), \boldsymbol{\Delta})\cdot\boldsymbol{u}_0 \tag{B.5}$$

The reason to use the formulation above for an uncertain, linear system, as in the case of a vessel with RRS, is that the robust stability and performance checks may be performed in a straightforward manner. But first, the robust stability and performance problems must be set into perspective. For introducing the concepts, the formulation of Eq. (B.3) will be used with no loss of generality, as the second of Eq. (B.5) guarantees that any conclusions can be extended to the case where a controller is present by substituting $\boldsymbol{P}$ by $\boldsymbol{F}_\ell(\boldsymbol{P}, \boldsymbol{K})$.

In this respect, robust stability of uncertain linear plants may be guaranteed in an H_∞-norm framework, provided that the "size" of the perturbation $\boldsymbol{\Delta}$ does not exceed the following upper bound.

$$\|\boldsymbol{P}_{11}\|_\infty < \frac{1}{\gamma} \Longleftrightarrow \|\boldsymbol{\Delta}\|_\infty \leq \gamma \tag{B.6}$$

It is reminded here that the H_∞ norm of a multivariable linear system G is defined as follows.

$$\|G(s)\|_\infty \triangleq \sup_{\omega \geq 0} \sigma_{\max}(G(s = \mathrm{j}\omega)) \tag{B.7}$$

In the above, $\sigma_{\max}(\bullet)$ stands for the maximum singular value of a possibly complex matrix. The H_∞ norm is often referred to as the $\boldsymbol{L}_2$ to $\boldsymbol{L}_2$-induced norm due to the following fundamental property.

$$\|\boldsymbol{G}(\boldsymbol{s})\|_\infty = \max_{\|\boldsymbol{u}\|_2 < \infty} \left(\frac{\|\boldsymbol{y}\|_2}{\|\boldsymbol{u}\|_2}\right) \tag{B.8}$$

In the above, $\boldsymbol{u}$ is the input signal vector, $\boldsymbol{y}$ the output one, and $\|\bullet\|_2$ stands for the $\boldsymbol{L}_2$ norm (Euclidean norm).

If condition in Eq. (B.6) is met by any admissible perturbation $\boldsymbol{\Delta}$ in the specified set, then the perturbed nominal plant $\boldsymbol{P}$ is said to be robustly stable under any specified perturbation $\boldsymbol{\Delta}$. Several additional technical conditions (Skogestad and Postlethwaite 1996; Tempo and Blanchini 1996; Zhou and Doyle 1998) are also needed for the validity of the robust stability check given in Eq. (B.6); for example, the nominal plant $\boldsymbol{P}$ must be stable, if unperturbed. However, the test of Eq. (B.6) is significant and useful as it allows to determine the "maximum" perturbation that does not have a destabilizing effect to the perturbed closed-loop system.

A robust performance test is obtained by extending the robust stability criterion of Eq. (B.6). The extension requires the introduction of the structured singular value (SSV or μ) (Zhou and Doyle 1998; 1996). SSV allows to structure any uncertainty. Indeed, employing the notation above, the SSV of a complex matrix, $\boldsymbol{P}$, under the admissible perturbation set of, possibly complex, $\boldsymbol{\Delta}$'s, denoted $\mu_{\boldsymbol{\Delta}}(\boldsymbol{P}) = \mu_{\boldsymbol{\Delta}}(\boldsymbol{P}_{11})$, is the minimum value of the H_∞ norm of those perturbations $\boldsymbol{\Delta}$ that cause matrix $(\boldsymbol{I} - \boldsymbol{P}_{11}\boldsymbol{\Delta})$ to become singular, i.e., cause $|\boldsymbol{I} - \boldsymbol{P}_{11}\boldsymbol{\Delta}| = 0$; in the case that no such $\boldsymbol{\Delta}$ exists, then $\mu_{\boldsymbol{\Delta}}(\boldsymbol{P}) = 0$. It can be seen that the robust stability condition of Eq. (B.6) obtains the following form in the SSV framework.

$$\|\mu_{\boldsymbol{\Delta}}(\boldsymbol{P}(s))\|_\infty < 1 \text{ where } \|\mu_{\boldsymbol{\Delta}}(\boldsymbol{P}(s))\|_\infty \triangleq \sup_{\omega > 0} \mu_{\boldsymbol{\Delta}(s=\mathrm{j}\omega)}(\boldsymbol{P}(s = \mathrm{j}\omega)) \tag{B.9}$$

The manner to check robust performance is to convert this problem to a robust stability one and then apply Eq. (B.9). In literature, this is achieved by augmenting the original uncertainty block, $\boldsymbol{\Delta}$, by a generic, complex-valued one of appropriate dimensions, $\boldsymbol{\Delta}_0$, as shown in Fig. B1. Again, with no loss of generality, the conclusions will be presented with respect to the uncontrolled process $\boldsymbol{P}$ as they can be extended to the case where a controller is present by substituting $\boldsymbol{P}$ by $\boldsymbol{F}_\ell(\boldsymbol{P}, \boldsymbol{K})$. The objective is to obtain a feedback system without any exogenous inputs or outputs. Robust performance is guaranteed provided that the following condition is true.

$$\|\mu_{\hat{\boldsymbol{\Delta}}}(\boldsymbol{P}(s))\|_\infty < 1 \text{where } \hat{\boldsymbol{\Delta}} = \mathrm{diag}(\boldsymbol{\Delta}, \boldsymbol{\Delta}_0) \tag{B.10}$$

A prerequisite of the above to suffice is nominal performance, as given below without loss of generality.

$$\|\boldsymbol{P}(s)\|_\infty < 1 \text{ or, in the case of a controller present } \|\boldsymbol{F}_\ell(\boldsymbol{P}, \boldsymbol{K})\|_\infty < 1 \tag{B.11}$$

References

Balchen JG, Jenssen NA, Mathisen E, Sælid SA (1980) Dynamic positioning system based on Kalman filtering and optimal control. Model Identif Control 1(3):135–163. https://doi.org/10.4173/mic.1980.3.1

Bretschneider CL (1959) Wave variability and wave spectra for wind generated gravity waves. Technical report, beach Erosion board, corps, of engineers, 118

Christensen AC, Blanke M (1986) A linearized state-space model in steering and roll of a high-speed container ship. Technical University of Denmark, Servolaboratory, DTH, Copenhagen, 10–32

Cowley WE, Lambert TH (1972) The use of rudder as a aoll stabilizer. Proceedings of the 3rd international ship control systems symposium (SCSS'72), Bath, UK, 345–354

Doyle JC, Glover K, Khargonekar P, Francis B (1989) State-space solutions to standard H_2 and H_∞ control problems. IEEE Trans Autom Control 34(8):831–847

Eda H, Crane CL (1965) Steering characteristics of ships in calm water and in waves. Society of Naval Architects and Marine Engineers-Transactions 73:132–163

Faltinsen OM (1990) Sea loads on ships and offshore structures. Norwegian Institute of Technology, Trondheim, 257–277

Fossen TI (1994) Guidance and control of ocean vehicles. John Wiley and Sons, Tronheim, 295–306

Fossen TI (2011) Handbook of marine craft hydrodynamics and motion control. John Wiley and Sons, Tronheim, 433–445

Glover K, Doyle JC (1988) State-space formulae for all stabilizing controllers that satisfy an H_∞ norm bound and relations to risk sensitivity. Syst Control Lett 11:167–172

Golnaraghi F, Kuo BC (2010) Automatic control systems. Prentice-Hall, Vancouver, 253–275

Green M, Limebeer DJN (1995) Linear robust control. Prentice-Hall, London, 263–301

Healey AJ (1992) Marine vehicle dynamics lecture notes and problem sets. Naval postgraduate school (NPS), Monterey, 22–34

Kallstrom CG, Schultz WL (1990) An integrated rudder control system for roll damping and maintenance. 9th International Ship Control Systems Symposium (SCSS'90), Bethesda, MD, 9.228–9.296

Lauvdal T (1998) Stabilization of linear systems with input magnitude and rate saturations. PhD thesis, Norwegian University of Science and Technology, Trondheim, Norway, 87–96

Lloyd AEJM (1975) Roll stabilization by rudder. Proceedings of the 4th international ship control systems symposium (SCSS,75). Hague, Netherlands, 581–609

Martin RJ (1985) Multivariable control system design for a submarine using active roll control. Master thesis, MIT, Cambridge, Massachusetts, USA, 52–76

Nagrath IJ, Gopal M (1986) Control systems engineering, 2nd edn. John Wiley and Sons, Singapore, 513–568

Neumann G (1952) On wind-generated ocean waves with special reference to the problem of wave forecasting. New York University, College of Eng. Res. Div., Dept. of Meteorology and Oceanography, New York, 11–35

Perez T (2005) Ship motion control course keeping and roll stabilization using rudder and fins. Springer-Verlag, London, 113–122

Pierson WJ, Moskowitz L (1964) A proposed spectral form for fully developed wind seas based on the similarity theory of SA Kitaigorodskii. J Geophys Res 69(24):5181c5190. https://doi.org/10.1029/JZ069i024p05181

Roberts GN (1992) Ship roll damping using rudder and stabilizing fins. Proceedings of IFAC workshop on control applications in marine systems (CAMS'92), Genoa, Italy, 129–138

Saelid S, Jenssen NA (1983) Adaptive ship autopilot with wave filter. Model Identif Control 4(l):33–46. https://doi.org/10.4173/mic.1983.1.3

Skogestad S, Postlethwaite I (1996) Multivariable feedback control. Analysis and design. Wiley, Chichester, 253–290

Smith JE (1977) Mathematical modeling and digital simulation for engineers and scientists. John Wiley and Sons, New York, pp 175–203

SNAME (1989) The society of naval architects and marine engineers. Guide for Sea Trials Technical and Research Bulletin No 3–17

Son KH, Nomoto K (1981) On the coupled motion of steering and rolling of a high speed container ship. Nav Archit Ocean Eng 150:232–244. https://doi.org/10.2534/jjasnaoe1968.1981.150_23

Sorensen AJ, Sagatun SI, Fossen TI (1995) Design of a dynamic positioning system using model based control. IFAC Proceedings Volumes 28(2):16–26

Tempo R, Blanchini F (1996) Robustness analysis with real parametric uncertainty. Levine WS (ed) The Control Handbook. IEEE Press, 495–505

Triantafyllou MS, Bodson M, Athans M (1983) Real time estimation of ship motions using kalman filtering techniques. IEEE J Ocean Eng 8(l):9–20. https://doi.org/10.1109/JOE.1983.1145542

Van Amerongen J, Van Cappelle JC (1981) Mathematical modelling for rudder roll stabilization. Proceedings of the 6th International Ship Control Systems Symposium (SCSS'81), Ottawa, Canada, 238–260

Van Amerongen J, Van der Klugt PGM, Van Nauta Lempke HR (1990) Rudder roll stabilization for ships. Automatica 26(4):679–690. https://doi.org/10.1016/0005-1098(90)90045-j

Van Der Klugt PGM (1987) Rudder roll stabilization. Technische Universiteit Delft, Delft, 1–192

Zhou WW (1987) Identification of nonlinear marine systems. PhD thesis, The Technical University of Denmark, Servolaboratoriet, Lyngby, 97–143

Zhou K, Doyle JC (1998) Essentials of robust control. Prentice-Hall, Louisiana, 253–300

Zhou K, Doyle JC, Glover K (1996) Robust and optimal control. Prentice-Hall, 365–392